Aus der Klinik für Innere Medizin mit Schwerpunkt Kardiologie und Pulmologie der Medizinischen Fakultät Charité – Universitätsmedizin Berlin

DISSERTATION

The role of nucleotide-binding oligomerization domain containing protein 2 (Nod 2) in coxsackievirus B3 induced myocarditis in mice model

zur Erlangung des akademischen Grades
Doctor medicinae (Dr. med.)

vorgelegt der Medizinischen Fakultät
Charité – Universitätsmedizin Berlin

von

Yu Xia

aus China

Datum der Promotion: .....22.06.2014.....

CONTENTS

Summary

In the present study, the role of the pathogen-recognition receptor Nod2 in murine CVB3-induced myocarditis was investigated for the first time. In the study, Nod2 knockout mice and wild type (WT) mice were infected with CVB3. Seven days after infection, mice were hemodynamically characterized via a conductance catheter, and heart tissue was snap-frozen for subsequent determination of immunohistochemical and molecular biology parameters.

Hemodynamic analysis of pressure-volume data indicated that the reduction in global, systolic and diastolic function after CVB3 infection was less pronounced in Nod2$^{-/-}$ CVB3 mice compared to CVB3-infected WT mice. In agreement with these findings, molecular biology and immunohistochemical examination of the heart, showed a weaker inflammatory response in the myocardium of Nod2$^{-/-}$ CVB3 mice compared to the WT CVB3 mice. In brief, the CVB3-induced infiltration of macrophages, T, and B cells, as well as of CVB3-induced *TNF-α* and *IL-1β* mRNA expression was weaker in Nod2$^{-/-}$ CVB3 mice compared to WT CVB3 mice. Concomitantly, *MCP-1* mRNA expression was lower in Nod2$^{-/-}$ CVB3 mice compared to WT CVB3 mice, which might underlie the reduced cardiac infiltration of immune cells in Nod2$^{-/-}$ CVB3 mice versus WT CVB3 mice. Furthermore, Nod2$^{-/-}$ CVB3 mice manifested less cardiac fibrosis as indicated by lower CVB3-induced collagen I, III, and α-SMA expression, less cardiac apoptosis, and less viral load than the WT CVB3 mice.

These findings suggest a crucial role of Nod2 in the pathogenesis of CVB3-induced myocarditis: via the Nod2 downstream activation of NF-κB upon CVB3 infection, the cardiac expression of cytokines and chemokines such as TNF-α, IL-1β, and MCP-1 is induced, triggering the infiltration of immune cells into the heart, leading to cardiac fibrosis and cardiac apoptosis and to an increased viral load.

Zusammenfassung

In der hier vorliegenden Arbeit wurde die Rolle des Pathogen-Recognition Rezeptors (PPR) Nod2 in der murinen Myokarditis zum ersten Mal beschrieben.

Zu diesem Zweck wurden Nod2 Knockout ($Nod2^{-/-}$) Mäuse und Wildtyp (WT) Mäuse mit dem Coxsackie Virus B3 (CVB3) infiziert. Sieben Tage nach Infektion erfolgten die hämodynamische Charakterisierung der Herzfunktion, mittels Konduktanzkatheter, und die Entnahme des Herzens für immunhistochemische und molekularbiologische Untersuchungen.

Die Analyse der gewonnenen Druck-Volumen-Kurven zeigte, dass die Verringerung der globalen, systolischen und diastolischen Funktion nach CVB3-Infektion bei den $Nod2^{-/-}$-Mäusen, verglichen mit den WT Mäusen, weniger stark ausgeprägt war. Ergänzend dazu, konnte eine schwächere Entzündungsreaktion im Myokard der $Nod2^{-/-}$-CVB3 Mäuse im Vergleich zu den WT-CVB3 Mäusen detektiert werden. Dies spiegelte sich in einer geringeren Infiltration von Makrophagen, T- und B-Zellen, sowie einer geringeren mRNA-Expression von TNF-α und IL-1β wieder. Des Weiteren war die MCP-1 mRNA-Expression in $Nod2^{-/-}$-CVB3 Mäusen im Gegensatz zu den WT-CVB3 Mäusen reduziert, was in der verringerten kardialen Infiltration von Immunzellen begründet sein könnte. Auch manifestierte sich in $Nod2^{-/-}$-CVB3 Mäusen weniger Herzfibrose, assoziiert mit einer verminderten Expression an Kollagen I, III und α-SMA, weniger kardiale Apoptose und eine reduzierte Viruslast.

Insgesamt deuten diese Ergebnisse auf eine zentrale Rolle von Nod2 in der Pathogenese der CVB3 induzierten Myokarditis hin. Über die Aktivierung des NF-κB Signalweges durch Nod2 wird die kardiale Expression von Zytokinen und Chemokinen, wie TNF-α, IL-1β und MCP-1, induziert. Dies führt zu einer Infiltration von Immunzellen in das Herz, weiterhin zur Fibrose, Apoptose und zu einer erhöhten Viruslast.

Abbreviations and acronyms

α-SMA	alpha-smooth muscle actin
AD	acidic activation domain
APC	antigen presenting cells
ASC	apoptotic speck-containing protein
BIR	baculovirus inhibitor of apoptosis repeat
BLS	bare lymphocyte syndrome
CAR	coxsackie adenovirus receptor
CARD	caspase activating and recruitment domain
CINCA	chronic infantile neurologic cutaneous articular syndrome
CO	Cardiac output
CVB	group B coxsackievirus
DAF	decay accelerating factor
DCM	dilated cardiomyopathy
dP/dt_{max}	Maximum LV pressure rise
dP/dt_{min}	Minimum LV pressure decay rate
EBDs	effector-binding domains
EF	Ejection fraction
HR	Heart rate
HCV	hepatitis C virus
HIV	human immunodeficiency virus
IFN	interferon
IKK	inhibitor of NF-κB kinase
JAK	Janus kinase
LPS	lipopolysaccharide
LRRs	leucine-rich repeats
LVPmax	Maximum left ventricular pressure
LVEDP	End-diastolic left ventricular pressure
LVEDV	End-diastolic LV volume

LVESP	End-systolic left ventricular pressure
LVESV	End-systolic LV volume
MAVS	mitochondrail antiviral signaling
MCP	Monocyte chemotactic protein
MHC	major histocompatibility complex
MIP	Macrophage inflammatory protein
MDP	muramyl dipeptide
NACHT	domain present in NAIP,CIITA,HET-E, and TP-1
NAD	NACHT-associated domain
NeoR	neomycin resistance
NK	natural killer
NOD	nucleotide-binding oligomerization domain
PAMPs	pathogen-associated molecular patterns
PGN	peptidoglycan
PRRs	pathogen-recognition receptors
PYD	pyrin domain
RSV	respiratory syncytial virus
SOCS	suppressor of cytokine signaling
ssRNA	single-strand positive-sense RNA
STAT	Signal Transducer and Activator of Transcription
SV	Stroke volume
TK	thymidine kinase
TLRs	"Toll-like" receptors

1.Introduction

1.1 Myocarditis

1.1.1 Definition

Myocarditis is defined as the inflammation of the cardiac tissue mostly caused by viral infections and less commonly by other pathogens (bacteria and parasites), toxic or hypersensitivity drug reactions[1, 2]. It is accompanied by a wide range of symptoms from mild dyspnea or chest pain to cardiogenic sudden death and dilated cardiopathy. From the mid-eighties of the last century, a histological method, the standard Dallas histopathological criteria, were used for defining myocarditis. It requires that an inflammatory cellular infiltrate with necrotic cardiomyocytes is detected on conventionally stained heart-tissue sections [3]. Currently, based on new medical knowledge in relation to the understanding of immunological processes of human body and the conduct of animal studies, the diagnosis of myocarditis has been extended by additional immunohistochemical, molecular biological methods using imaging detection [4] (Figure 1). The detection of myocarditis can be carried out by immunoperoxidase staining in greater sensitivity [5]. According to the definition of the world organization for heart disease ("World Heart Federation"), active myocarditis is quantitatively defined as an infiltration of >14 lymphocytes±macrophages per mm^2 accompanied by simultaneous necrosis and edema [6].

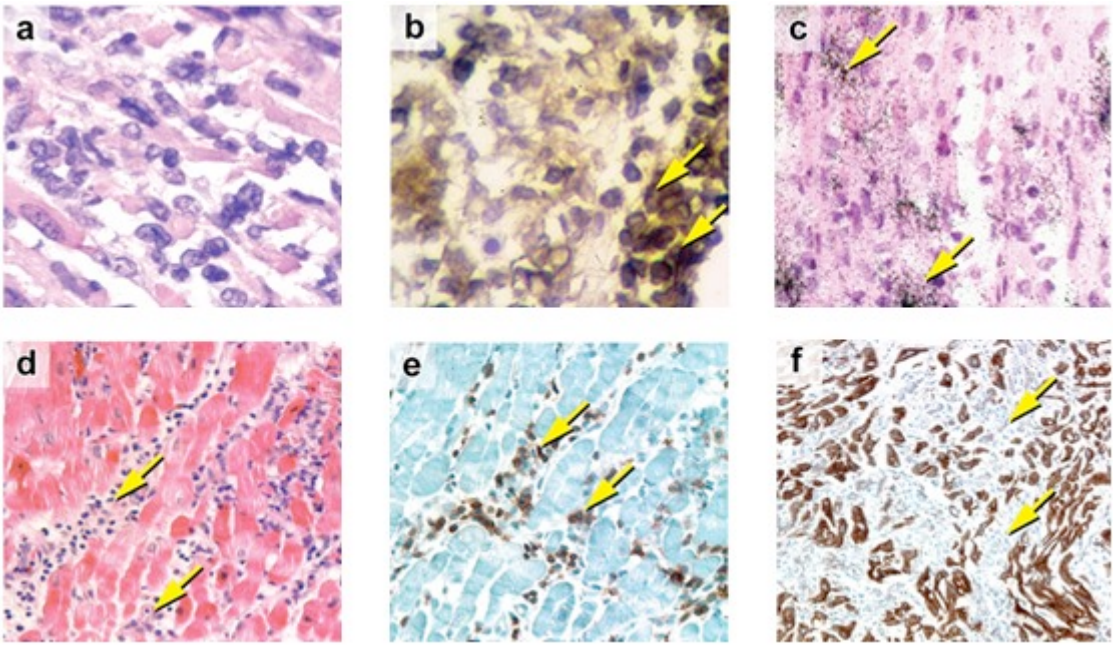

Figure 1. Histopathological manifestation of myocarditis in heart tissue sections from patients with acute myocarditis. Heart sections (*a*–*c*) are from a nine-day-old female with fulminant viral myocarditis. Panel *a*

(original magnification 400×) shows inflammatory mononuclear cells and edema, damaged myocytes, and Panel *b* (original magnification 400×) shows positive leukocyte-common-antigen (LCA) (*arrows*). Panel *c* (original magnification 200×) shows positive-strand viral RNA (*arrows*) in the myocardium detected by radioactive *in situ* hybridization. Heart sections (*d–f*) are from a 54-year-old female with viral myocarditis. Immune infiltrates (*arrows*) are evident on H&E staining (*d*; original magnification 400×). Macrophages (*arrows*) are stained positively with anti-CD68 (*e*; original magnification 400×). A significant loss of cardiac myocytes and disruption of myocardial architecture (*arrows*) are shown with HHF35 staining (*f*; original magnification 200×). CD68, antibody marker for monocytes and macrophages; HHF35, antibody against muscle actin. Modified from Esfandiarei *et al*. [7].

1.1.2 Epidemiology

It is difficult to determine the exact incidence of myocarditis due to the variable symptoms, sometimes asymptomatic in the clinic, and the lack of widely available and accurate noninvasive diagnostic methods [8, 9]. The use of endomyocardial biopsies, which were for the first time used in the late 1970s instead of post-mortem studies, remain the gold standard for diagnosis in living patients with myocarditis now [10]. The incidence is estimated around 0.1-10 persons per 100,000 members of the population [11]. The prevalence of myocarditis in autopsies is considered to be from one to five percent. Pathological examination shows that 8.6% of sudden cardiac deaths among young adults are due to myocarditis [12].

1.1.3 Etiology

The emergence of myocardial inflammation can be attributed to a variety of potential causes. The most common cause are viral pathogens, involving Group B of coxsackievirus and other enteroviruses, adenovirus [13], parvovirus B19 [14], hepatitis C virus [15], human immunodeficiency virus (HIV) [16] and influenza virus [17]. Interestingly, there is a different geographical distribution of the virus prevalence: the prevalent viruses in North America are the enteroviruses, in Western Europe, the parvovirus B19 and the more common virus in Japan is the hepatitis C virus (HCV). Among all of these, coxsackie viruses are traditionally regarded as the dominant pathogen, especially for babies and young children [7].

Coxsackieviruses are a sub-classification of the family of *Picornaviridae* of human enteroviruses. They are divided into two groups (A and B) [18]. The group A coxsackievirus was reported by

Dalldorf and Sickles in 1948 from a case of febrile paralysis in the town of upstate New York named Coxsackie[19], and the group B coxsackievirus (CVB) was discovered shortly thereafter [20]. Six serotypes of CVB (CVB1-6) are known, of which only CVB1-5 circulate commonly in the United States and Northern/Western Europe. Humans are the natural host of CVB. The primary transmission of the coxsackievirus is fecal-oral or by droplet infection[21].

1.1.4 Clinical course and prognosis

The clinical presentation of viral myocarditis varies from completely asymptomatic in the majority of patients to acute heart failure with left ventricular dysfunction. Cardiac symptoms may be fatigue, decreased exercise tolerance, chest pain, palpitations and syncope. In newborns and adolescents, acute forms are more common and usually present in multi-organ dysfunction, whereas in adults, it is milder with only a small percentage of patients with fulminant myocarditis [22, 23].

Nevertheless, there are different forms of disease in adult patients: patients with mild cardiac dysfunction usually recover completely [24]. Patients with severe disease and left ventricular dysfunction have a poorer prognosis: at least one third of them will approach chronic heart failure, approximately 25% will die or need cardiac transplantation [25]. A recent study also found differences between genders. Men with myocarditis were found to have a significantly worse recovery and a lower transplant-free survival rate than women [26].

Myocarditis is divided into 4 types according to clinical and histopathological criteria [7, 27]:

- Fulminant myocarditis: characterized by LV dysfunction and heart failure within 2-3 weeks after a viral infection;
- Subacute myocarditis: characterized by moderately impaired LV function and non-specific symptoms;
- Chronic active myocarditis: characterized by moderately impaired LV function and non-specific symptoms. Endomyocardial biopsies show a persistent inflammation, myocardial damage and active formation of scar tissue;
- Chronic persistent myocarditis: characterized by normal LV function and atypical symptoms. Persistent inflammation can be demonstrated by biopsies.

The progress of this disease is unpredictable and varies widely: patients who survive from acute

myocarditis can recover completely, or their condition may deteriorate into dilated or constrictive cardiomyopathy [7].

1.1.5 Animal models of myocarditis

A number of experimental animal studies, particularly performed in murine models owing to the availability of transgenic strains and sensitivity to cardiotropic viruses, shed light on the function of the specific genes in myocarditis and the relationship between the extent of immune responses and the severity of disease.

Usually, following intraperitoneal (i.p.) injection of CVB3, three pathological phases of myocarditis can emerge successively: acute phase (0-3 days post-infection), subacute phase (4-14 days after infection), chronic phase (from 15 days post infection). In the acute phase, day 3 to 4 post infection, a high titer of virus is detected in the blood and myocardium accompanied by histological changes in the form of focal dying of myofibers (both necrotic and apoptotic), multivesicular vacuolation, and calcification in the absence of myocardial inflammatory infiltrates [28, 29]. Furthermore, an increased content of myocardial mRNA levels of proinflammatory cytokines such as TNF-α, IL-6, IL-1β and interferon-γ (IFN-γ) [30], as well as an increased incidence of neutralizing antibodies, which play critical roles in limiting viral replication[31], is detected. In the subacute phase, the phase of disease which evolves with the release of progeny virus into the interstitium, which results in the migration of natural killer (NK) cells and macrophages to the tissue of injury followed by a considerable increase of proinflammatory cytokines and a second wave of infiltration of immune cells including antigen-specific CD4+ and CD8+ T lymphocytes. Virus infection is expanded with the development of multifocal inflammatory lesions. Direct viral injury and host immune responses determine the severity of the acute to subacute phases. Ultimately, in the chronic phase, the progeny viruses in the blood and peripheral tissues are completely cleared. Alternatively, continual viral replication and immune cell infiltration still persist in the heart, which is believed to be responsible for further progress of viral myocarditis to dilated cardiomyopathy (DCM) and congestive heart failure.

1.2 Pathophysiology of myocarditis

Our present understanding of myocarditis is based on experimental data of animal studies and of human cardiac biopsies [32, 33]. The experimental data are mainly from murine models in which myocarditis is caused by group B coxsackieviruses. The group A coxsackieviruses, with 23 known serotypes, mainly infect immature mouse muscle cells and causes widespread myositis accompanied by flaccid paralysis [21], while the group B, containing six known serotypes (1-6), is associated with various diseases, such as myocarditis, type 1 diabetes mellitus, pancreatitis, and aseptic meningitis. Three serotypes of group B coxsackieviruses (CVB1, CVB3, CVB5) are proved with cardiovirulence [34, 35]. The CVB3 serotype has been identified in several studies as the predominant cause of myocarditis and is associated with about 20-40% of acute myocarditis or DCM [36, 37]. The genome of CVB3, as all picornaviruses, is a 7.4-kb ssRNA comprising a large open reading frame with untranslated regions on both 3' and 5' termini. At the 5'end, the usual eukaryotic 7-methyl guanosine cap structure is replaced by a small virus-encoded protein, VPg (3B) [38].

The development of the disease is controlled by the interaction between the virus and the immune system, but the actual mechanisms of pathogenesis remain controversial. There are two suggested mechanisms [7]:

- direct virus-induced myocardial injury
- Immune response-mediated injury

1.2.1 Viral entry and direct CVB3-induced myocardial injury

The viral entry of coxsackievirus usually happens in the gastrointestinal tract. The primary infected organs and systems include the lymph nodes, spleen, and the pancreas. Two hours after viral entry, the virus can be detected at these sites [39]. Further, virus replication takes place and the distribution of the virus infection occurs in the secondary target organs, such as the liver, brain and heart, through the blood circulation and lymphatic system.

Virus replication emerges initially in the secondary lymphoid organs such as the spleen and lymph node, and is identified by the macrophages, the B lymphocytes and T lymphocytes. This suggests that these immune cells are the main carriers of virus to the infected end organs of the host [40]. Based on the biological interactions between the virus and the host cell, the virus will

be stabilized in the germinal center of the lymph nodes. Then, the B lymphocytes are infected and the viral infection expands into the further organs [41].

In the heart and the other organs, the CVB3 receptors or receptor complexes are used to penetrate the cells. The main receptor for this process is the coxsackie adenovirus receptor (CAR) [39], which has been proved in studies of CAR knockout mice with CVB3 infection [42, 43]. CAR belongs to the immunoglobulin family. It includes an extracellular domain, which is necessary for viral infection, a transmembrane α-helical domain, and a cytoplasmic tail [44]. It has adhesion properties [40] and is associated in human epithelial cells with tight junctions. In human tissues, CAR is present in the heart, pancreas, brain, prostate, liver and intestine, which is consistent with the pattern of tissue susceptibility and clinical characteristics in CVB3-induced myocarditis [45, 46]. Another membrane protein, the decay-accelerating factor (DAF), is also involved in CVB3 binding and entry to the cell. DAF, a 70 kDa membrane protein, is widely expressed in human tissues [47] and interacts with $p56^{lck}$ kinase, which plays a crucial role in CVB3-induced myocardial injury [48]. Nevertheless, the expression profile of DAF as such is not enough to explain the tropism of all the tissues in experimental mouse models, which suggests the possibility of existence of other factors and receptors that play a role in viral entry and replication [49] [50].

The direct virus-induced injury, caused by viral proteases, has been documented by numerous studies indicating that virus replication results in myocardial cell death during the early phase of myocarditis prior to immune cell infiltration [29, 51-54]. By binding to the CAR, viral RNA enters into the cell cytoplasm following the attachment, internalization, and virus uncoating. Then, the transcription and thereby the production of the viral proteins starts by using viral positive-sense RNA as a template. Following post-entry translation, several proteases are released within the cytosol, which subsequently induce the cleavage of cellular proteins, which are necessary for cellular homeostasis (Figure 2). Viral proteases further contribute to the cleavage of cytoskeletal proteins such as dystrophin and the dystrophin-associated glycoproteins α-sarcoglycan and β-dystroglycan, leading to cardiomyopathy. Data from animal models also indicate that CVB may persist in the myocardium with a partially deleted genome, which may induce low-grade, non-cytolytic and chronic infection in the heart followed by chronic DCM [55].

1.2.2 Immune response

The immune response against CVB3 is complex and consists of different mechanisms of the innate and antigen-specific immune system. A specific immune response against CVB3 is generally necessary to eliminate the virus completely. Before the specific immune response becomes fully active in humans 7-14 days after primary infection, few mononuclear cell infiltrates are determined in the heart 4-5 days post viral infection, in the early stages of infection, while a substantial virus infection in cardiomyocytes starts from 3 days after infection [56]. Moreover, an increase in virus-specific IgG is detected from 7 days after CVB3 infection [57]. This indicates that the innate immune system plays an important role in the first 5-7 days post CVB3 infection in mice.

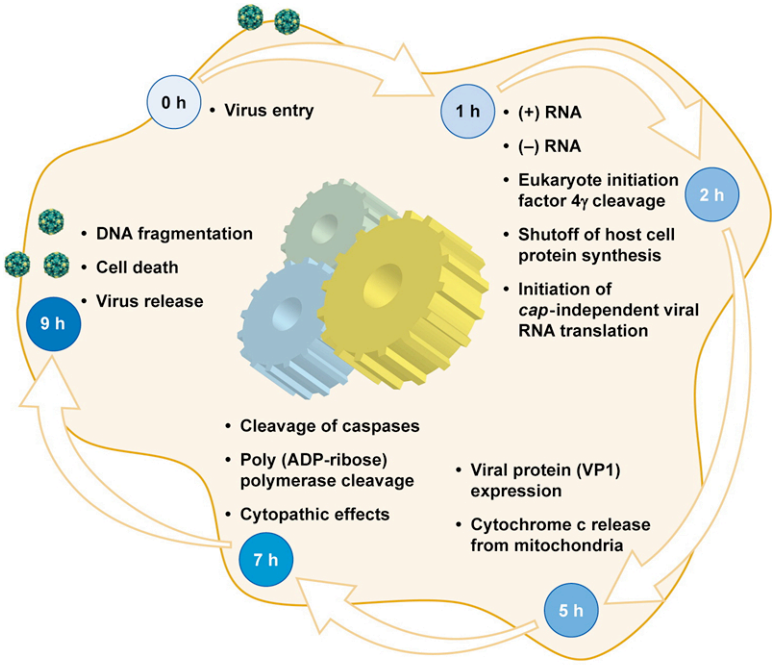

Figure 2. Direct cell damage caused by the coxsakievirus. In a cell culture model of coxsackievirus infection, the viral RNA is produced 1-2 hours after infection. Viral proteases cleave "host" cell proteins, leading to the elimination of the translation of the "host" RNA. Viral proteases further cleave proteins of the transcription and the cytoskeleton, resulting in cytopathic phenotype and morphological changes. The expression of viral proteins is followed by the release of cytochrome c from mitochondria and results in cleaving the caspase family and subsequent cytoplasmic and nuclear damage. Then, apoptotic events can be detected and progeny

viruses are released into the vicinal tissues. From Esfandiarei *et al*. [7].

1.2.2.1 Innate immune response

Toll-like receptors in innate immune response after CVB3 infection

The innate immune response is an immediate counterattack after entry of the virus. This process is initiated by pathogen-recognition receptors (PRRs) recognizing pathogen-associated molecular patterns (PAMPs). So far, two families have attracted attention: the "Toll-like" receptors (TLRs), the best characterized PRRs, and the nucleotide-binding oligomerization domain (NOD)-like receptors. To date, 13 murine TLRs and 10 human TLRs have been identified [58], among which the subtypes TLR4, TLR7 and TLR8 are believed to be mainly involved in CVB3 sensing mechanisms since the viral replication is significantly reduced in the absence of TLR4[59] and the expression of TLR7/8 receptors significantly increases during CVB3 infection. They can recognize synthetic imidazoquinoline-like molecules and single-strand RNA (ssRNA) [60] and activation of TLR7 signaling was also found inducing autophagy [61]. TLR7 may recognize CVB3 ssRNA through the fusion between endosomes and autophagosomes, which seems to serve as a platform of CVB3 replication. Finally, activation of these receptors induces the activation of a variety of pro-inflammatory cytokines, adhesion molecules and chemokines by intracellular signal transduction [62]. These active molecules coordinate the migration of immune cells into the site of inflammation resulting in myocardial injury.

Cytokine in innate immune response of myocarditis

Cytokines are a family of signal-transfer molecules, which are proteins or glycoproteins. They are produced by various cells, both hematopoietic and non-hematopoietic cells. Particularly, they are expressed by immune cells activated by a pathogen. Their main role is to modulate systemic immunity of the body, acting as the first line of defense against virus infection since they can recruit and activate immune cells. Their effect is either pro- (IL-1, IL-6, IL-12, TNF-α, interferons), or anti-inflammatory (IL-4, IL-10) and is exerted by binding to specific receptors. The signals of these receptors lead to a up or down-regulation of genes and transcription factors, and attracting immune cells to the site of inflammation.

Cytokines play a crucial role in CVB3 myocarditis. During the acute phase after infection, viral

particles of CVB3 are detected by the TLRs on the macrophages (CD68+ cells) and other antigen presenting cells (APC). With the signals of different TLRs, cytokines, including IL-1, IL-6, IL-12, IL-18, TNF-α, TNF-ß, and interferon-γ (IFN-γ), are produced subsequently. IFNs, which are regarded as potent and pivotal antiviral cytokines in mammals, are secreted by the infected cells. Now, three types of IFNs are identified, these consist of type I IFN (mainly α/β), type II IFN (γ) and type III IFN (λ). Type I IFN plays a central role in innate antiviral immunity. It has been demonstrated in isolated adult mouse cardiomyocytes that type I IFNs(α/β) inhibits virus infection, while type II IFN(γ) showed no antiviral effects [63]. Type I IFNs also leads to the upregulation of major histocompatibility complex (MHC) class I and II antigens, which stimulate T-cells and NK cells, inhibit the cell cycle and initiate proapoptotic signals [64]. Their effects are critical for host protection and survival. Interestingly, the results of experiments only show that type I IFNs are crucial for limiting systemic viral replication after CVB3 infection, but whether endogenous type I IFNs can inhibit CVB3 in the heart remains unclear [65, 66].

In the study using cardiac-specific suppressor of cytokine signaling (SOCS) transgenic mice, the role of cytokine-mediated cardiac protection against CVB3 infection has been revealed [56, 63]. Many cytokines are known to activate transcription of the cytokine-responsive genes, including SOCS, through the JAK(Janus kinase) - STAT (Signal Transducer and Activator of Transcription) system [67]. SOCS family proteins are a negative-feedback regulator of JAK-STAT signaling by inhibiting JAK-mediated phosphorylation of the cytokine receptor and subsequently the activation of STAT signaling, which tightly regulates the duration and intensity of the cytokine-induced JAK-STAT system. It was also found that activation of JAK-STAT signaling induces the expression of *SOCS1* and *SOCS3* mRNA in the heart after CVB3 infection, which demonstrates the important role of JAK-STAT signaling within the cardiac myocyte in the prevention of CVB3 infection.

The cytokines, which are indeed necessary for normal immune response against CVB3, also have negative effects on the course and prognosis of myocarditis. In experimental mice with CVB3 induced myocarditis, administration of IL-1β and TNF-α resulted in increased myocardial inflammation and necrosis, as well as poor prognosis [68]. In *in vitro* studies, a direct cardiovascular depressor effect of TNF-α, IL-2 and -6 was indicated on isolated papillary muscles [69], whereas the same cytokines may also induce cardiac hypertrophy [70, 71].

Chemokines in innate immune response of CVB3-induced myocarditis

Chemokines are a family of small cytokines that are expressed by the tissue cells in the early phase of infection. They induce chemotactic activity of the immune cells located in the vicinity of infected cells at the site of inflammation. Chemokines, like cytokines, exert their effect through membrane-bound receptors. Their function is to bring leukocytes, monocytes, neutrophils and other effector cells from the bloodstream to the site of inflammation. Chemokines are distinguished into four groups according to the distance between their first two cysteine residues: CC, CXC, C, and CX3C.

During CVB3 infection, the upregulation of chemokines can be detected in the heart [49]. In CVB3 myocarditis, the "Macrophage inflammatory protein" (MIP) -1 and -2 (CCL3 or CXCL2), CCL5 (RANTES), and the "Monocyte chemotactic protein" (MCP) -1 (CCL2) are increased [4], while the expression of chemokines CCL2, CCL3, CCL4 and CCL5 emerge in CVB-induced pancreatitis [39]. The production of chemokines in the myocardium during CVB3 myocarditis is not always beneficial to the outcome of the disease: MIP-1 and -2, and CCL5 exert negative effects, attracting T cells against the patient's cardiac antigens [72-74]. Experimental overexpression of MCP-1 in the heart leads to myocarditis by increasing the inflammatory activity in the myocardium [75]. In a clinical study in patients with DCM, increased expression of MCP-1 was observed, which was potentially due to a direct negative impact of increased monocytes on the cardiomyocytes [76]. Another chemokine, fractalkine (CX3CL1), seems to play an important pathogenic role in the adaptive immune response in experimental autoimmune myocarditis in rats [77]. Husberg *et al*., demonstrated an induction of fractalkine by IL-1β and IFN-γ in human heart failure, as well as in experimental heart failure, whereby an increase in the inflammatory response was induced by the fractalkine [78]. Therefore, chemokines can, by induction of a strong inflammatory reaction in the myocardium, strengthen the adverse effects on the course of the disease.

Effector cells in the innate immune system:

The NK cells and the "natural killer" T cells (NK T cells) are the main effector cells of the innate immune defense, which kill virus-infected cardiomyocytes in an attempt to limit virus

dissemination in CVB3-induced myocarditis [79]. These cytotoxic cells play a protective role in limiting CVB3 replication, which is found from NK-deficient mice, in which viral titers in the heart and pancreas and myocardial injury increase compared to control CVB3-infected mice [80] [81]. This effect is performed by the release of cytotoxic molecules such as perforin within the myocardium. In perforin heterozygous (+/–) and homozygous (–/–) knock-out mice, a lower level of myocardial necrosis and lymphocyte infiltration was found on day 12 after CVB3 viral inoculation [82].

1.2.2.2 Specific immune response

The specific immune response, in contrast to the immediate reaction to the virus by the innate immune response, will take typically days or weeks. T and B cells are responsible for the specific nature of the adaptive immune response. They can recognize particular epitope sequences from the virus with high affinity and selectivity via various receptors.

Role of B cells:

The production of neutralizing antibodies by B cells is important for the elimination of the CVB3. Such antibodies appear about 4 days after the infection in the murine model, and play a critical role in the limitation of virus replication [31]. Patients with congenital agammaglobulinemia, which are genetically incapable of antibody production, show a susceptibility to chronic infections by coxsackieviruses and enteroviruses. B cell "knockout" mice show a chronic CVB3 infection with a high viral titer and DCM [41]. B cells are also found to be infected in the early phase of the infection by the CVB3, which raises the possibility that these cells may play the role in virus's ability to establish or disseminate infection [83].

Role of T cells:

T cells play a two-sided role in CVB3 infection. The elimination of the virus in mice without a thymus is impaired [84]. Experimental murine models of CVB3-induced myocarditis without CD4+, CD8+ T cells, or both, were used to reveal the role of these cells in the pathogenesis and tissue damage of myocarditis [99]. The elimination of CD4+ T cells had a beneficial effect on

the disease, while the elimination of CD8+ T cells had a negative effect, and the elimination of both cell types led to the greatest protection against myocarditis. It was also found that the exact role of the T cells can vary between the various strains of mice [85].

These results show that the specific cellular immune response can protect the "host" from CVB3 myocarditis on the one hand, and can significantly contribute to the pathology on the other hand.

1.3 NOD-like receptors (NLRs)

In the past decade, research of innate immunity has found that its activity relies on many microbial sensors, PRRs, which can recognize conserved microbial motifs from bacteria and viruses known as PAMPs [86]. The first family of PRRs attracting considerable interest was the TLR family [87]. The function of TLRs in innate immunity is supported by a rich and dense literature. However, recent studies have provided insights into the presence of surveillance mechanisms against bacteria in the cytosol [88], while the TLRs recognize PAMPs in extracellular compartments or at the cell surface. This indicated the possibility that other receptors were involved in the host response to pathogens. NLRs, a group of the intracellular PRRs, are believed to be one of them. NLRs are particularly necessary given the high incidence of genetic variations in various immune diseases. 23 members of NLRs are found in humans [89] and four subfamily designations have been approved based on the N-terminal domain: 1) NLR family, acidic domain containing (NLRA); 2) NLR family, BIR domain containing (NLRB); 3) NLR family, CARD domain containing (NLRC);4) NLR family, pyrin domain containing (NLRP) [90] (Table 1).

1.3.1 NOD-like receptors function

1.3.1.1 Recognition of PAMPs

The most prominent function of NLRs is to sense the structures shared by microbes and endogenous molecules, which include *lipopolysaccharide (LPS)*, a component of the cell wall of Gram-negative bacreria, *peptidoglycan (PGN)*, common in practically all bacteria, *flagellin*, the structural component of bacterial flagella, *zymosan*, a component of the cell wall of yeast, and ssRNA from viruses [91]. The structure of most NOD proteins includes variable amino-terminal effector-binding domains (EBDs), which are involved in downstream signaling, a central

nucleotide-binding oligomerization domain (NBD, also known as the NACHT) and carboxy-terminal leucine-rich repeats (LRR), which is involved in the sensing of ligands [92]. Through the LRR, NLRs recognize exogenous (derived from microorganisms) and endogenous ligands ("danger signals") resulting in self-oligomerization and subsequent regulation of downstream effector molecules through the EBDs [93].

1.3.1.2 NLRs signaling

Until now, two well-documented signaling pathways of NLRs have been discovered, an inflammasome-dependent pathway for NALPs, Ipaf and Naip, and a NF-κB pathway for NOD1 and NOD2.

Many PAMPs, recognized by NLR-dependent pathways, induce the activation of the inflammasome, an endogenous multi-protein signaling complex composed of ASC (apoptotic speck-containing protein with a CARD), caspase-1 and caspase-5, resulting in the recruitment and activation of caspase-1, pro-IL-1β and pro-IL-18 [94]. NALPs, Ipaf and Naip family members have been discovered participating in this pathway with three distinct inflammasomes (NALP1 inflammasomes, NALP3 inflammasomes and Ipaf inflammasomes).

On the other hand, NOD1 and NOD2 are found to induce immune responses through the NF-κB pathway. After detection of peptidoglycan, NOD1 and NOD2 form self-oligomerization and then transiently interact with receptor-interacting protein 2 (RIP2), also named RICK or CARDIAK, via its CARD domain [95]. The role of RIP2 is supported by one study, in which NOD1 and NOD2 cannot activate NF-κB expressed by mouse embryo fibroblasts from RIP2-deficient mice, but NF-κB is reactivated after exogenous addition of RIP2 [96]. The NOD1-RIP2 (or NOD2-RIP2) complex then recruits the inhibitor of NF-κB kinase (IKK) complex, which induces activation of NF-κB and further secretion of pro-inflammatory cytokines.

Table 1. New Approved Designations for the Human NLR Family Members

NLR Family	HGNC-Approved Symbol	Other Names and Aliases	Domain Organization
NLRA	CIITA	MHC2TA;C2TA,	(CARD)-AD-NACHT-NAD-LRR;
NLRB	NAIP	NLRB1;CLR5.1;BIRC1	BIR3x-NACHT-LRR;
NLRC	NOD1	NLRC1; CARD4; CLR7.1	CARD-NACHT-NAD-LRR;
NLRC	NOD2	NLRC2;CARD15;CD;BLAU; IBD1;PSORAS1;CLR16.3	CARD2x-NACHT-NAD-LRR
NLRC	NLRC3	NOD3;CLR16.2,	CARD-NACHT-NAD-LRR
NLRC	NLRC4	CARD12 ;CLAN; CLR2.1; IPAF,	CARD-NACHT-NAD-LRR
NLRC	NLRC5	NOD27; CLR16.1,	CARD-NACHT-NAD-LRR
NLRP	NLRP1	NALP1;DEFCAP; NAC;CARD7; CLR17.1,	PYD-NACHT-NAD-LRR-FIIND-CARD
NLRP	NLRP2	NALP2;PYPAF2;PAN1; NBS1; CLR19.9	PYD-NACHT-NAD-LRR
NLRP	NLRP3	CIAS1;PYPAF1;Cryopyrin;CLR1.1; NALP3	PYD-NACHT-NAD-LRR
NLRP	NLRP4	NALP4;PYPAF4;PAN2; RNH2; CLR19.5	PYD-NACHT-NAD-LRR
NLRP	NLRP5	NALP5;PYPAF8;MATER; PAN11;CLR19.8	PYD-NACHT-NAD-LRR
NLRP	NLRP6	NALP6;PYPAF5;PAN3; CLR11.4	PYD-NACHT-NAD-LRR
NLRP	NLRP7	NALP7;PYPAF3;NOD12; PAN7; CLR19.4	PYD-NACHT-NAD-LRR
NLRP	NLRP8	NALP8;PAN4;NOD16; CLR19.2	PYD-NACHT-NAD-LRR
NLRP	NLRP9	NALP9;NOD6;PAN12; CLR19.1	PYD-NACHT-NAD-LRR
NLRP	NLRP10	NALP10;PAN5; NOD8;PYNOD; CLR11.1	PYD-NACHT-NAD
NLRP	NLRP11	NALP11;PYPAF6;NOD17; PAN10; CLR19.6	PYD-NACHT-NAD-LRR
NLRP	NLRP12	NALP12;PYPAF7;Monarch1;RNO2;PAN6;CLR19.3	PYD-NACHT-NAD-LRR
NLRP	NLRP13	NALP13;NOD14;PAN13; CLR19.7	PYD-NACHT-NAD-LRR
NLRP	NLRP14	NALP14;NOD5;PAN8; CLR11.2	PYD-NACHT-NAD-LRR
NLRX	NLRX1	NOD9;CLR11.3,	X-NACHT-NAD-LRR

Modified from Jenny P. Y. Ting *et al.* [90].

1.3.1.3 NLRs in the innate immune response

Most evidence about NLRs involvement in immune responses is reported from bacteria studies. The detection of NOD1 against invasive *S. flexneri* in cultured epithelial cells represents the first demonstration that NLRs are involved in sensing a bacterial PAMP [97]. Moreover, studies have revealed the importance of NOD1 in the cytosolic recognition of Gram-negative bacterial invasion and NOD2 in innate immune responses to intracellular infection by Gram-positive pathogens[98, 99], which also indicate the function of NLRs as essential cytosolic signal transducer of innate immune responses to invasive bacterial infection. After recognition of bacteria by NLRs, several upregulated proinflammatory factors are detected in the host cell, which are believed to recruit inflammatory cells essential in bacteria clearance. The release of proinflammatory cytokines (such as TNF-α, IL-1β and IL-6) by monocytes is detected upon stimulation with NOD1- or NOD2-activating agonists, as well as the induction of chemokine IL-8 upon stimulation of epithelial and myeloid primary cells [100-102]. Furthermore, several studies show that several members of the NLRs are involved in processing of the cytokines IL-1α, IL-1β and IL-18 by the inflammasome-dependent pathway [103]. Otherwise, NLRs are supposed to be the cytoplasmic counterparts of TLRs to constitute the cellular defense within the cell. Several recent studies give insights into the possible synergy between NOD and TLR by using macrophages isolated from NOD-deficient animals. The results indicate that NOD1 and NOD2 are dispensable for TLR signaling [92, 104]. Conversely, in the study by Watanabe *et al.* [105], a negative role of NOD2 on TLR2-mediated induction of IL-12 and IFN-γ in a subpopulation of murine splenocytes (CD11b+ cells) has been shown. Additionally, there is evidence that TLR and NOD ligands act in synergy. For example, stimulation of MDP, a ligand of NOD2 and NLRP3, upregulates MyD88 expression and MDP-stimulated macrophages induce a significant increase of *TNF* mRNA translation and release, which is enhanced by LPS costimulation. Therefore, the molecular basis of the synergistic effect between TLRs and NLRs remains to be explored. Further research of NLRs function and identification of additional ligands is needed to clarify such discrepancies.

1.3.2 NLRs in human diseases

The implication of NLRs linkage to human immunological diseases is indicated by disease-based gene studies, thus providing further information of their role *in vivo*. Mutations in MHC2TA, which encodes CIITA, are found to induce type II bare lymphocyte syndrome (BLS) [106]. Patients with BLS suffer from immunodeficiency because of the absence of MHC class II molecules, which are responsible for the activation of T cell and host defense against pathogens. Additionally, mutations in Cias 1 (encodes NLRP3) are associated with autosomal dominant disease, including familial cold autoinflammatory syndrome (or familial cold urticaria), Muckle-Wells syndrome, and neonatal onset multisystem inflammatory disease (also known as chronic infantile neurological cutaneous articular syndrome, CINCA) [92, 93, 107]. Recently, mutations in Card4 (encodes NOD1) have been found to be associated with increased susceptibility to asthma and inflammatory bowel disease (IBD) [108, 109]. In both cases, the mutations are known as an insertion deletion polymorphism in an intron of NOD1. And in asthma, this mutation is linked to augment IgE level despite the presence or absence of allergen-specific IgE. Moreover, mutations in Card15 (encodes NOD2) are associated with disease characterized by granulomatous inflammation, such as Crohn disease [110], Blau syndrome [111] and early-onset sarcoidosis [112]. Gene alternations in Crohn disease are mapped to the LRR region of NOD2, while Blau syndrome and early-onset sarcoidosis link to missense point variant in the region of NACHT domain. All of them are associated with enhanced NF-κB activity.

1.3.3 NOD2

NOD2 is a well-characterized member of the NLR family. It was identified by Ogura Y *et al.* in the early 2000s [95] and characterized by two N-terminal CARDs, a central NACHT, and a LRR in C-terminal end. The expression of NOD2 seems to locate mostly in myelomonocytic cells (monocytes/macrophages, granulocytes), dendritic cells and intestinal epithelial cells [95, 113] and the subcellular distribution of NOD2 has proved elusive. Besides its cytosolic location, it is also found in the plasma membrane of epithelia and monocytes [113, 114].

1.3.3.1 NOD2-dependent pathways in response to bacterial infection

Most studies of NOD2 are based on its response to bacterial infection. It can recognize the PGN fragment MurNAc-L-Ala-D-isoGln called muramyl dipeptide (MDP), which is found in both

Gram-negative and Gram-positive bacteria. After sensing MDP, whose mechanism remains unclear, NOD2 then undergoes an auto-oligomerization process, which results in the exposure of the CARD domain, and induces subsequently the RIP2 recruitment through homotypic CARD-CARD interactions. This NOD2-RIP2 complex then binds to IKKγ, inducing the activity of NF-κB (Figure 3). In antigen-presenting cells, this pathway contributes to the NOD2-mediated inflammatory and immune response by secreting proinflammatory cytokines (IL-6, TNF-α, IL-β, IL-10,IL-18, IL-12) and chemokines (IL-8, MIP2, MCP-1).

NOD2 has also been found to play a role in the host defense against bacteria by autophagy. Recent findings provide evidence that NOD2 is implicated in MDP-induced autophagy in non-myeloid cells (fibroblasts and epithelial cells) or myeloid monocytes (macrophages) [115-117]. These studies demonstrate that NOD2-induced autophagy by a mechanism independent of classical NF-κB signaling, requiring the autophagy regulator ATG16L1 [116], which is recruited to infection sites with NOD2. Based on these studies, it is proposed that the role of NOD2 in autophagy is to serve as a molecular scaffold for nucleation of autophagy machinery.

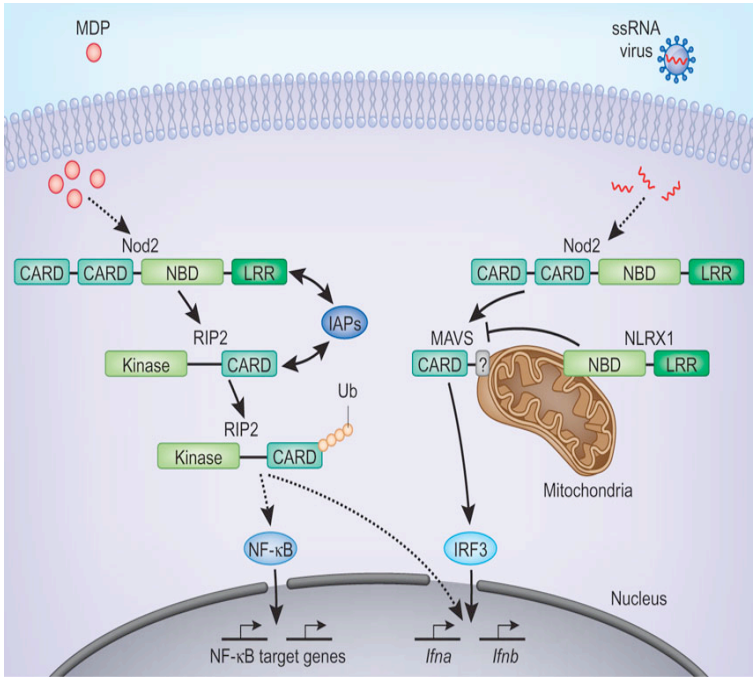

Figure 3. Two distinct pathways of NOD2 activation. The first MDP-induced pathway, initiated from the plasma membrane, involves the inhibitor of apoptosis proteins (IAPs) and the kinase RIP2; the latter becomes

ubiquitinated (Ub) and subsequently activates NF-κB, leading to inflammatory gene expression. The second pathway involves ssRNA virus-induced activation of NOD2, initiated from the mitochondria, leading to IRF3 activation and interferon gene expression after binding with MAVS. Modified from Peter J Murray [118].

1.3.3.2 NOD2-mediated pathways in response to viral infection

The role of NOD2 as PRR recognizing MDP, one of PAMPs, has been proved by a rich and dense literature. However, so far, no data have shown direct NOD2-MDP binding. Recent studies have indicated that NLRX1, which has the same NACHT and LRR domains as NOD2, interacts with the mitochondrail antiviral signaling (MAVS) protein and subsequently leads to the downregulation of the interferon pathway and the formation of reactive oxygen species [119, 120]. In addition, NOD2 is found to induce the formation of human β-defensin 2 with stimulation of MDP. Human β-defensin 2 is also upregulated in human cells after infection with respiratory syncytial virus (RSV), which is a paramyxovirus with ssRNA genome [121, 122]. These findings evoke interest whether NOD2 recognizes ssRNA to induce inflammation and immune response against viruses, which will expand the function of NOD2 beyond detection of peptidoglycan. Sabbah *et al.* found that NOD2 could be activated after infection of viruses containing an ssRNA genome, including RSV, vesicular stomatitis virus (VSV), or influenza virus [123]. Activation of NOD2 would lead to IRF3-dependent IFN-β secretion and antiviral immunity. Further investigation demonstrated that the MAVS extinction impaired NOD2-dependent IFN-β production after RSV infection. Consistent with the study of NLRX1 mentioned above, it is believed that NOD2-dependent IFN-β production in response to ssRNA involves the mitochondrial adaptor MAVS, which subsequently recruits downstream signaling complexes for IRF3 and NF-κB activation (Figure 3). Altogether, it opens the avenues for the multifaceted role of NOD2 in virus detection instead of being a dedicated receptor for MDP recognition.

1.4 Objectives

The prominent functions of NLRs, in particular NOD2, are sensing ssRNA in the immune response to virus infection. So far, the role of NOD2 in myocarditis, induced by the ssRNA virus CVB3, has not been unravelled. However, the genome of CVB3 is also known as a ssRNA. But the role of NOD2 in CVB3-induced myocarditis is even less well understood so far. In this study, experimental CVB3-induced myocarditis NOD2 "knockout" mice are applied to answer the following questions regarding the role of NOD2 in CVB3-induced myocarditis:

- Does NOD2 deficiency bring about a change of the cardiac phenotype after viral infection with CVB3?
- Is the change in the cardiac phenotype associated with a dysfunction of the cardiac hemodynamic in CVB3 myocarditis?
- Is there a change in apoptosis of cardiac cells due to NOD2 deficiency during CVB3 myocarditis?
- Does NOD2 deficiency exert an effect on cardiac viral load after CVB3 infection?
- What is the change induced by NOD2 deficiency in the cardiac inflammatory response to viral infection with CVB3?
- Do potential changes of the cardiac phenotype, the viral load, the rate of apoptosis of cardiac cells, the extracellular matrix and cardiac inflammatory responses by NOD2 deficiency have an impact on the survival after CVB3 infection?

2. Materials and methods

In the following part of the study, the materials and methods used in the study of relevance of Nod2 in CVB3-induced myocarditis in murine animal model are presented.

2.1 Materials

Table 2. Consumption materials

Article	**Description**	**Company**
MicroAmp®Optial 384-well plate	Reaction plate with Barcode	Applied Biosystems, Darmstadt, Germany
96-well Multiply®-PCR plate		Sarstedt, Nürnbrecht, Germany
Coverslips	21 x 26mm	R.Langenbrinck, Emmendingen, Germany
Cryotubes	1.5ml	Greiner, Solingen-Wald, Germany
Falcon tubes	15ml, 50ml	Sarstedt, Nürnbrecht, Germany
Folded filter	MN615 1/4·¢240mm	Macherey-Nagel, Düren, Germany
Gloves		Sempercare, Northamptoshire, Germany
Masks		Charite, Berlin, Germany
Microtome blades	A35 type	Feather, Köln, Germany
PCR-tubes	0.2ml, conical lid	Biozym, Hess. Oldendorf, Germany
Pellet pestle + tubes	Dstry-SR-15 + 1.5ml tubes	Biozym, Hess. Oldendorf, Germany
Pipette tips	10µl,100µl,200µl,1250µl	Sarstedt, Nürnbrecht, Germany
Pipettes		Biozym, Hess. Oldendorf, Germany
Plastic cannulas	18G und 20G	Braun, Meisungen, Germany
Reaction Tubes	Safe-Lock or RNAse free	Sarstedt, Nürnbrecht, Germany
Scalpels		Feather, Köln, Germany
Slides	Super Frost Plus	R.Langenbrinck, Emmendingen, Germany

Table 3. Laboratory equipments

Equipment	**Description/Type**	**Company**
Conductance catheter	1.2 French	Scisense Inc., Ontario, Canada
Cryostat		Microm, Minnestota, USA
Freezer -20 °C	Economic super	Bosch AG, Stuttgart, Germany
Freezer -80 °C	Nuaire Ultralow Freezer	Zapf Instrumente, Sarstedt, Germany
Homogenizer	Pellet Pestle Motor	Sigma, Taufkirchen, Germany
Horizontal shaker	SM-25	Edmund Bühler, Tübingen, Germany
Ice maker	AF-10	Scotsman, Vernon Hills, USA
Incubator	Function Line	Heraeus, Osterode, Germany
Microscope	DMRBE	Leica, Bensheim, Germany
P-V Amplifier System	MPVS 300/400	Millar Instruments, Houston, USA
pH meter	Knick Digital 646	Beyer, Düsseldorf, Germany
Pipettes		Eppendorf, Wesseling-Berzdorf, Germany
Spectrophotometer	NanoDrop	Thermo Scientific PEQLAB, Erlangen, Germany
Thermomixer	Comfort	Eppendorf, Wesseling-Berzdorf, Germany
Thermocycler	Mastercycler gradient	Eppendorf, Wesseling-Berzdorf, Germany
Tabletop centrifuge	Centrifuge 5415 C	Eppendorf, Wesseling-Berzdorf, Germany
Ventilator	Mini-Vent	Harvard Apparatus, Massachusetts,USA
Vortexer	VF2	IKA-Labortechnik, Staufen, Germany

Table 4.Buffer and reagent

Article	**Company**
1%ß-mercaptoethanol	Sigma, Taufkirchen, Germany
3-amino-9-ethylcarbazole(AEC)	Sigma, Taufkirchen, Germany
Anti-α-SMA	Abcam, Cambridge, Germany
ABC-Kit	Vector Labs, Burlingame, USA
Acetic acid	VWR Merck, Darmstadt, Germany
Acetone	VWR Merck, Darmstadt, Germany
Avidin-Biotin-Blocking-Kit	Vector Labs, Burlingame, USA
Bovine serum albumin	Vector Labs, Burlingame, USA
BSA	Roth, Karlsruhe, Germany
Calcium chloride	VWR Merck, Darmstadt, Germany
Anti-CD3+	Santa-Cruz Biotechn, Heidelberg, Germany
Anti-CD4+, 11b+	BD Bioscience, Heidelberg, Germany
Anti-CD68+	Bioss, Freiburg, Germany
Anti-Collagen I (secondary antibody)	Chemicon, Nuernberg, Germany
Anti-Collagen III (secondary antibody)	Calbiochem, Darmstadt, Germany
DeadEnd™ Colorimetric TUNEL System	Promega, Mannheim, DE
DNAse I	Qiagen, Hilden; Germany
Dianova (secondary antibody)	Dianova, Hamburg, Germany
Distilled water	Delta Select, Pfullingen, Germany
EnVision K4003	Dako, Hamburg, Germany
Ethanol	Sigma, Taufkirchen, Germany
EDTA	VWR Merck, Darmstadt, Germany
FCS	PAA, Cölbe, Germany
Formalin	Sigma, Taufkirchen, Germany

Gene expression assay	Applied Biosystems, Darmstadt, Germany
High Capacity Archive Kit	Applied Biosystems, Darmstadt, Germany
Hemalum	VWR Merck, Darmstadt, Germany
Hydrogen peroxide	Sigma, Taufkirchen, Germany
Isopropanol	Sigma, Taufkirchen, Germany
Kaiser's glycerol gelatin	VWR Merck, Darmstadt, Germany
Magnesium chloride	VWR Merck, Darmstadt, Germany
Mcp-1	Abnova, Aachen, Germany
N, N-dimethylformamide	Roth, Karlsruhe, Germany
Potassium chloride	VWR Merck, Darmstadt, Germany
Potassium dihydrogen phosphate	VWR Merck, Darmstadt, Germany
RNeasy Mini Kit	Qiagen, Hilden; Germany
RNase-free water	Applied Biosystems, Darmstadt, Germany
High Capacity cDNA Reverse Transcription Kit	Applied Biosystems, Darmstadt, Germany
TaqMan®Gene Expression Master Mix(2×)	Applied Biosystems, Darmstadt, Germany
Sodium acetate	VWR Merck, Darmstadt, Germany
Sodium chloride	VWR Merck, Darmstadt, Germany
Sodium hydrogen phosphate	VWR Merck, Darmstadt, Germany
Tris-Base	Sigma, Taufkirchen, Germany
Tris-HCl	VWR Merck, Darmstadt, Germany
TRIzol Reagent	Invitrogen, Karlsruhe, Germany
Tissue Tek	Sakura, Zoeterwoude, Netherlands

2.2 Methods

2.2.1 Study design

"Knockout" mice are a very good model to illuminate the role of specific gene products in various diseases by preventing the expression of this gene. In this study, male Nod2 "knock out" (-/-) mice, in which the Nod2 gene was deleted, were used.

Six-week-old C57BL/6 wild-type mice (WT) and $Nod2^{-/-}$ mice with a genetic background of C57BL/6 from the Institute of Microbiology Charité – Universitätsmedizin Berlin (Berlin, Germany) were used. Mice were randomly divided into 4 groups (Table 5).

Table 5. Groups of mice in the study

Animal phyla	**Group**	**Number**
Wild-type control	WT	6
$Nod2^{-/-}$ control	$Nod2^{-/-}$	7
Wild-type CVB3 infected	WT CVB3	9
$Nod2^{-/-}$ CVB3 infected	$Nod2^{-/-}$ CVB3	9

WT mice (WT CVB3) and $Nod2^{-/-}$ mice ($Nod2^{-/-}$CVB3) were infected with 5 x 10^5 plaque-forming units (p.f.u.) of CVB3 ("Nancy strain") via intraperitoneal (i.p.) injection at day 0. The corresponding control animals were injected with an identical volume of saline (0.2 ml) instead of CVB3. Seven days after infection, mice were anesthetized and the hemodynamical function of the heart was measured by conductance catheter. All mice were then sacrificed. The hearts and lungs were removed and weighed. The left ventricle was isolated from the atria and right ventricle, and divided into 4 pieces, which were quickly frozen in liquid nitrogen for molecular and immunohistochemistry examination later by using "real-time" PCR and immunohistochemistry, respectively.

The experimenters followed the guidelines of the U.S. National Institute of Health, USA-"Guide for the Care and Use of Laboratory Animals", published by the U.S. National Institutes of Health (NIH Publication no. 85-23 revised, 1985).

2.2.2 Mouse strains

Nod2$^{-/-}$ mice and WT (C57BL/6) mice were provided by the Institute of Microbiology Charité – Universitätsmedizin Berlin (Berlin, Germany).

For these "knockout" mouse strains, the corresponding genes (in this case the gene segment for Nod2) were isolated. First of all, a special vector containing no-function targeted gene sequence, the neomycin resistance (neo^{R}) and the thymidine kinase (TK) selectable markers was constructed. Then, this targeting construct is transported into mouse embryonic stem cells. Due to its homologous ends with the target gene, it replaces the target gene on the chromosome by homologous recombination. Via neomycin resistance and gancyclovir sensitivity, the cells with the correct non-functioning gene sequence are selected. These cells are injected into 3.5-day-old mouse blastocysts and subsequently used in pseudo-pregnant mice. After this procedure, chimeric mice are generated. They are bred to obtain offsprings that are heterozygous for the knockout allele. Finally, after crossing, homozygous mice are generated with a “deleted” target gene from heterozygous offspring.

2.2.3 Characterization of hemodynamic function

2.2.3.1 Narcotic

Barbiturate thiopental (Glaxo-Smith) was used at a dose of 125 µg/kg body weight and administered by a single i.p. injection. The depth of anesthesia was checked by a painful stimulus. If necessary, additional 10% of the initial dose of narcotic was added.

2.2.3.2 Intubation and ventilation

All mice were fixed in supine position on a surgical platform. Their necks were put in hyperextension position. Under visual control, the animals were intubated with a 22G cannula as tracheal tube and mechanically ventilated by a ventilator (MiniVent, Harvard Apparatus, Massachusetts, USA) with respiratory rate of 200 units/min and stroke volume of 6.5 ml/kg body weight.

2.2.3.3 Record of left ventricular pressure-volume curves by conductance catheter

Seven days after infection by CVB3, all animals were subjected to a pressure-volume conductance catheter measurement under general anesthesia. In this investigation, the pressure and volume data of the left ventricle were recorded mathematically in real time volume graphs and the corresponding working diagram of the heart with conductance catheter. Using the same method, it is possible to determine both volume-dependent and -independent parameters that describe the heart pump function. In the experiments, a 1.2 French catheter (Scisense Inc., Ontario, Canada) was used to determine pressure and volume in the left ventricle. The catheter was connected to a pressure-volume-amplifier system (MPVS 300/400, Millar Instruments, Houston, USA). The data were collected using the software program "IOX", 1.8.9 (EMKA Technologies, Falls Church, USA) and then analyzed using the program "Circlab 2004" (Paul Steendijk, GTX Medical Software, Belgium). All recording systems and software programs were obtained using a PC equipped with "Windows XP" (Microsoft Corporation, USA).

“Open chest” approach was used in this study. A continuous transversal skin incision was made with scissors 2mm below the ribs from right side to left side until the diaphragm was clearly visible from beneath. If necessary, the vessels would be coagulated to avoid large blood loss. The diaphragm was then cut transversely and the pericardium was removed gently by forceps to expose the heart. The apex of the heart was punctured once with a 26G needle. Following this step, conductance catheter was inserted quickly into the puncture site. The placement of the catheter should be adjusted to obtain rectangular-shaped pressure volume loop. But in ill animals this shape of loop may not be rectangular.

A transverse incision was performed also in the neck from the distal region of sternocleidomastoidea to dexter of Trigonum clavipectorale to expose the jugular vein. Further, a 26G needle, which connected with a Hamilton precision syringe via a polyethylene hose previously filled with 10% sodium chloride solution, was inserted into the vein.

2.2.3.4 Theoretical background of conductance catheter study

The volume change of the blood pool within the LV chamber is changed to the electrical resistance. With the help of a catheter, the conductance is measured to calculate left ventricular volumes.

The conductance catheter consists of a pressure sensor and four electrodes, two above and two below the pressure sensor. An electric field with constant current is generated from the outer and inner electrodes to measure the potential difference. During the cardiac cycle, the physiological modification of left ventricular volume changes the resistance and the conductance of the blood. Thus the inner electrodes measure the changing potential difference. The volume V(t) in the left ventricle is described by the following formula:

$$V(t)=1/\alpha\times(L^2/\sigma)\times G(t)- V(c)$$

Where α is a gain coefficient (volume correction/calibration factor), L is the distance between the electrodes, σ is the conductivity of blood, G (t) is the measured total conductance at any time and V (c) is a correction volume due to the parallel conductance.

The electric field generated by the conductance catheter is not only through the blood, but also through the various adjacent tissues. The conductance obtained during measurement presents itself as a total conductance of blood and tissues (tissue of the left ventricle, the right ventricle, the pulmonary tissue, fat tissue, etc.). Thus, the calculated volume is overestimated. This effect is referred to as parallel conductance or parallel resistance. It must be carefully converted to correct volumes, which is formed by subtracting the V(c) caused by parallel conductance. Vc is calculated by the formula:

$$V(c)=1/\alpha\times(L^2/\sigma)\times G(p)$$

G (p) is the conductance of the muscle wall and the surrounding tissue (parallel conductance).

Two methods are generally used to determine G (p):

- Method I- Removing the blood from the left ventricle. Then, the current flows only through the surrounding tissues, and the measured conductance corresponds to the parallel conductance.
- Method II- Injecting 10% saline solution into the left ventricle. The data of the end-systolic volume (LVESV) and the end-diastolic volume (LVEDV) are marked during the change of conductance. Regression of the dots results in a linear function. The value of the intersection of the line, where LVESV = LVEDV = 0, is the desired V (c).

In this study, we prefer using method II. Approximately 10µl of a 10% saline solution was injected as a bolus into the jugular vein.

2.2.3.5 Protocol for characterizing the hemodynamic function

To minimize artifacts caused by breathing, the pressure-volume curves of the test animals were collected in the short-term status of apnea. All measured data were calculated as the mean of three measurements.

Evaluation of the base pumping function of the left ventricle ("steady state")

Receiving the pressure-volume curves in the condition of apnea for approximately five seconds. This procedure was performed three times.

Determination of the parallel conductance ("SAL")

Receiving the pressure-volume curves during the bolus injection of 10 µl saline (10%) through the closed infusion system and in a state of apnea for about five seconds. A total of three repetitions of this process were performed.

Occlusion of the inferior vena cava ("VCO")

Obtaining the pressure-volume curves during the total occlusion of the inferior vena cava by a vascular clamp and in a state of apnea for about five seconds. Three repetitions of this procedure were performed.

2.2.3.6 Parameters for global cardiac function

Heart rate (HR)

It is expressed in beats / min.

End-systolic LV volume (LVESV)

The volume of the left ventricle at the end of systole. It is expressed in µl.

End-diastolic LV volume (LVEDV)

The volume of the left ventricle at the end of diastole. It describes the end-diastolic differentiation of the heart as being the same as the end-diastolic LV pressure (LVEDP).

Stroke volume (SV)

The stroke volume describes the blood volume pumped from the left ventricle into the aorta with each beat. It is expressed in µl.

Calculation: subtraction of the end-systolic (LVESV) from the end-diastolic (LVEDV) volume

$$\mathbf{SV = LVEDV - LVESV}$$

Ejection fraction (EF)

It is the fraction of blood volume pumped out of the ventricles in each beat or cardiac cycle. It is

stated as a percentage:

$$\mathbf{EF= (LVEDV - LVESV)/ LVEDV \times 100}$$

Cardiac output (CO)

It is calculated by multiplying the stroke volume by the heart rate, and describes the total blood volume, ejected from the left ventricle into the aorta each minute. It is stated in µl/min.

2.2.3.7. Parameter for the systolic function

Maximum left ventricular pressure (LVPmax)

The maximum pressure generated by the left ventricle provides a meaningful measure of LV systolic function and is expressed in mmHg.

End-systolic left ventricular pressure (LVESP)

The pressure in the left ventricle at the end of the systole provides a meaningful measure of the left ventricular systolic function. This pressure corresponds to the end-systolic arterial pressure. It is expressed in mmHg.

Maximum LV pressure rise (dP/dt_{max})

It is a parameter for the systolic function, and specifically the contractility of the left ventricle. It is calculated mathematically from the first derivative of the left ventricular pressure curve and describes the maximum speed of the pressure rise in the LV. It is measured in mmHg/s.

2.2.3.8. Parameters for the diastolic function

Minimum LV pressure decay rate (dP/dt_{min})

The minimum rate of pressure change during the isovolumic relaxation is a scientifically verified parameter during early relaxation of the left ventricle. It is measured in mmHg/min.

Tau (τ)

Tau is a major parameter of early LV relaxation and represents the exponential decay of the ventricular pressure during isovolumic relaxation. The longer tau means a longer relaxation process of LV and a defective diastolic function. It is expressed in ms and shown by the following exponential function

$$\mathbf{P=P_0 \times e^{\,t/\tau} + P_\infty}$$

P = LV pressure,

P_0 = LV pressure at dP / dtmin,

t = time after dP/dtmin,

τ = Tau, time constant of the LV pressure decrease,

P_∞ = asymptote of the LV pressure when V=0 in the LV.

End-diastolic left ventricular pressure (LVEDP)

It is one of the most important parameters of diastolic function. It is measured at the end of the diastole of the left ventricle. Its increase shows impaired diastolic function and high load in the left ventricle. It is given in mmHg.

2.3. Molecular methods

2.3.1 RNA extraction

RNA isolation was performed by using the TRIzol® reagent from Invitrogen. The subsequent purification of the isolated RNA was performed with the aid of a RNeasy® Mini kit and a DNA digestion from Qiagen. The company's protocols were slightly modified.

Left ventricular tissues were taken out of liquid nitrogen and put into a 1.5 ml tube with 400 ìl TRIzol® Reagent. Then, the tissues were homogenized in TRIzol® reagent with a pellet pestle motor until no obvious tissue was present. In addition, the samples were supplemented with another 400 µl TRIzol® and mixed. The specimens were then incubated over a period of 10 minutes at 1000 rpm at room temperature in a thermomixer. Following incubation, 160 µl of chloroform was added per sample. The tubes were shaken vigorously by hand for 15 seconds and vortexed 10 seconds at a maximum of 1400 rpm. After that, the tubes were centrifuged at 12,000 g for 15 minutes at 4°C. After the centrifugation, the mixture was separated into three phases: a lower red phenolchloroform phase, a white interphase and a colorless upper aqueous phase, where RNA remained. The upper aqueous phase was carefully transferred without disturbing the interphase into a fresh 1.5 ml tube. To get a precipitation of the RNA, 400 µl of 100% isopropanol was added to the samples and incubated for a period of 10 minutes at room temperature. The expected gel-like pellets of RNA were obtained from the bottom of the tube by centrifugation for 10 minutes at 4°C with an acceleration of 12,000 g. The supernatants were removed completely and the pellets were dried for a few minutes and dissolved with 100µl-RNase-free water. The RNA was then mixed with a 350 µl RLT buffer with 1%

â-mercaptoethanol and 250 µl of 100% ethanol. All liquid was moved from the tube to the column of the RNeasy® Mini Kit from the company Qiagen. The RNeasy Mini columns were centrifuged for 15 seconds at 9,300 g at room temperature and subsequently washed with the buffer RW1. Each sample was mixed with 80 µl DNase I-Mix (10 µl DNase I + 70 µl buffer RDD) and incubated for 15 minutes at room temperature at 9300 g. Then, the column was infused with 350 µl wash buffer RW1 and centrifuged for 15 seconds at 9300g at room temperature. After that, 500 µl of RPE buffer was applied with subsequent centrifugation for 2 minutes at room temperature at 9300 g. In the next step, the flow-through was discarded, and the column was again centrifuged for one minute at room temperature and 9300g to dry the filter of the column. The spin column was subsequently moved from the collection tube to a new 1.5 ml tube and 40 µl of RNase-free water was added. The samples were incubated at room temperature for 5 minutes. Finally, the RNA was eluted via centrifugation at 16,100 g for 1 minute at room temperature.

To determine the concentration of RNA in the samples, 1 µl solution of each sample was examined using a spectrophotometer (NanoDrop) (Thermo Scientific PEQLAB, Erlangen, Germany). The software program is NanoDrop-1000 v3.1.2. The ratio from A260 to A280 was considered to assess the quality of isolated RNA.

2.3.2 Reverse transcription

A "High Capacity cDNA Reverse Transcription Kit", from Applied Biosystems, Darmstadt, Germany, was used to obtain a reverse transcription from the isolated mRNA into complementary DNA (cDNA). 1 µg of RNA was added to a total volume of 10 µl with RNase-free water.

The reaction tubes were incubated for 10 minutes at 70°C in the thermocycler. Meanwhile, a 2×Master-Mix was prepared by adding appropriate volumes of the following components to one tube: 2 µl 10×RT-Buffer + 0.8 µl 25×dNTP-Mix + 2 µl 10×Random-Primer) (Table 6), RNase-free water 4.2 µl, and reverse transcriptase 1 µl. The reaction tubes were then put directly on ice and mixed with 10 µl of the 2×Master-Mix. The transcription of RNA to cDNA was performed in a thermocycler according to the following program:

- room temperature for 10 min
- 37˚C for 2 hours
- 4 ˚C

Finally, 80 µl RNase-free water was added to each tube to dilute the cDNA 1:5 for the following PCRs.

Table 6. Primers used in the TaqMan® PCR

Primers	**Gen-"Assay-ID"**
Bax	Mm00432050_m1
Bcl2	Mm00477631_m1
CCL2	Mm99999056_m1
Col1a1	Mm01302043_g1
Col3a1	Mm00802331_m1
Foxp3	Mm00475156_m1
IFN-β	Mm00439546_s1
IFN-gamma	Mm00801778_m1
IL-1β	Mm00434228_m1
IL-10	Mm00439616_m1
IL-12a	Mm00434165_m1
MMP2	Mm00439505_m1
MMP9	Mm00442991_m1
RorC	Mm03682796_m1
TGF-β	Mm00441724_m1
TIMP-1	Mm00441818_m1
TNF-α	Mm00443258_m1

2.3.3 Real-time polymerase chain reaction

The TaqMan real-time PCR was carried out by using the reagents from "Applied Biosystems", Darmstadt, Germany. There is 10µl mix in each well of a 96-well plate (Table 7). Each cDNA sample was pipetted into two wells for the duplicate determination of the expression. All primers

were labeled with the dye FAM.

Table 7. Mix of TaqMan® PCR

Component	**1 Reaction**
TaqMan gene expression assay (20× forward, reserve primers and probes)	0.5 µl
cDNA	1 µl
TaqMan Universal PCR Master Mix (2×)	5 µl
Nuclease-free water	3.5 µl
Final volume	10 µl

The following procedure was used for the amplification of the sample with the 7900HT "Fast Real-Time" PCR system, of which steps 3 and 4 were repeated in cycles of 40 times:

- Prevention of carry-over contamination by addition of Uracil-DNA N-Glycosylase (UNG) for 2 minutes at a temperature of 50°C
- Denaturation and activation of the amplification-Taq DNA polymerase for 10 minutes at a temperature of 95°C
- Denaturation for 15 seconds at a temperature of 95°C
- Annealing and elongation for 60 seconds at a temperature of 60°C

The relative quantification of the collected data was performed using the SDS program 2.2.2 (Applied Biosystems, Darmstadt, Germany). The C_T values (the "threshold cycle" indicated the number of cycles in which a linear increase of the reporter fluorescence was detected over the baseline for the first time) of the endogenous reference (18S RNA) and the target sequence were determined. In each duplicate, an average of two C_T values was calculated (Figure 4).

Finally, the values (ΔC_T value) were normalized by subtracting the C_T values of the 18S gene ($C_{T(18S)}$) from the values of target gene ($C_{T(T)}$) (Figure 4):

$$\Delta C_T = C_{T(T)} - C_{T(18S)}$$

Then the expression values (E*v*) of the particular target gene was calculated according to the following formula:

$$Ev = 2^{-\Delta CT}$$

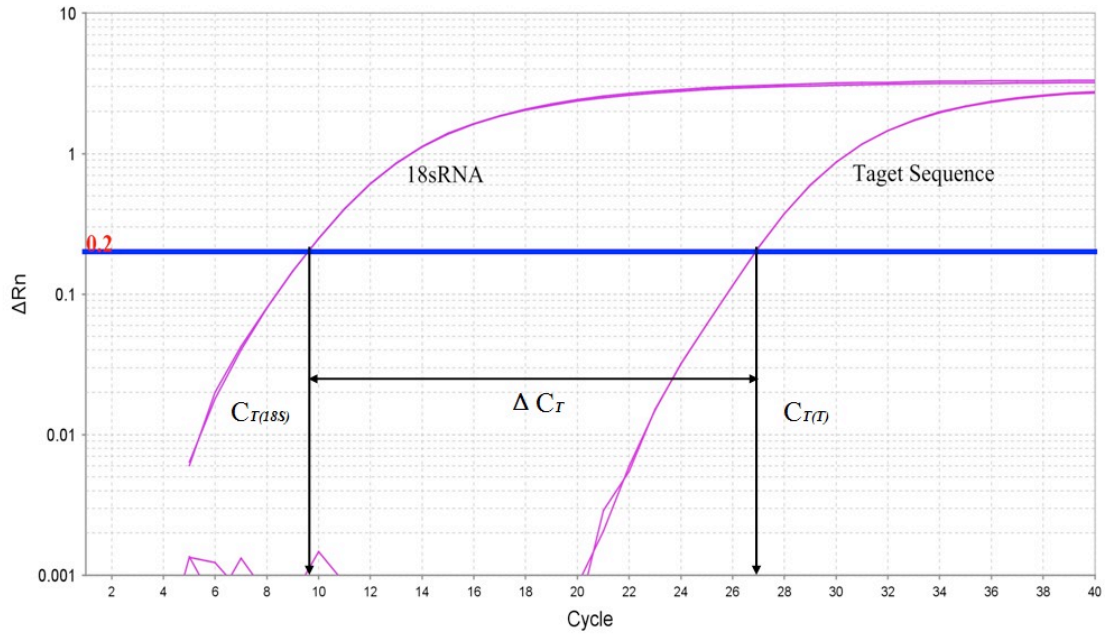

Figure 4. Determination of gene expression by calculating the $\Delta C_{T.}$

2.3.4 Determining the viral load

The viral number of copies in animal cardiac tissue was determined by using TaqMan® PCR to detect the viral load of the infected animals. Specific "forward" (5'-CCCTgAATgCggCTAATCC) and "reverse" (5'- ATTgTCACCATAAgCAgCCA) primers and a FAM-labeled TaqMan probe (5'FAM-TgCAgCggAACCg-3´) was used to determine the exact number of CVB3 copies in this study (Table 8). Standard dilutions of astandardized plasmid containing CVB3 (10^6 copies/µl, 10^5 copies/µl, 10^4 copies/µl, 10^3 copies/µl, 10^2 copies/µl and 10 copies/µl) served as a standard curve for accurate quantification of the copies of CVB3.

Table 8. Primers, probe, and preparation of the mixture to determine the number of CVB3 copies

	Conc.	**Volume**	**Company**
Universal PCR-master Mix	2×	5 µl	ABI
"Forward"-primer	60 ng/µl	0.5 µl	TIB-Molbiol
"Reverse"-primer	60 ng/µl	0.5 µl	TIB-Molbiol
MGB-TaqMan probe	5 pM/µl	0.5 µl	ABI
Nuclease-free water		1.5 µl	ABI
cDNA/Plasmid		2 µl	
Total volume		10 µl	

CVB3=coxsackievirus B3, *Conc*.=Concentration, *ABI*=Applied Biosystems, Darmstadt Germany, *TIB Molbiol*, Berlin Germany.

2.4 Immunohistochemistry

2.4.1 Generation of frozen sections

The tissue samples of the heart, which had been previously preserved at -80°C, were embedded in the snap-freeze unit using Tissue-Tek OCT compound (Sakura, Zoeterwoude, NL). Five-micron-thick frozen sections were prepared using the cryostat (Microm, Lobal Medical Instrumentation, Minnesota, USA).

Usually, six sections were placed on one slide, so that different layers of the heart muscle were located on the slide. Subsequently, the sections were immersed in ice-cold acetone for ten minutes. After drying, the slides were used immediately or stored at -20°C.

2.4.2 Theoretical background of immunohistochemical staining

The principle of immunohistochemical staining is based on antigen-antibody reaction, and its aim is to detect histological antigens on sections (Table 9). The antigen-specific antibody was bound by a secondary antibody with a coupled enzyme. Further, the distribution and localization of biomarkers or differentially expressed proteins in different parts of the tissue is then

visualized subsequently using the appropriate substrate. In this work, two methods were used: the Avidin-biotin complex (ABC) method and the EnVision® method.

Table 9. Antibodies for the immunohistochemical studies of cardiac tissue

Pri. Ab	**Species**	**Dilution**	**Sec.Ab**	**Species**	**Dilution**	**Method**
α-SMA	Rabbit	1:200	EnVision	Anti-Rabbit	—	EnVision
CD3+	Goat	1:75	ABC-Kit	Anti-Goat	1:250	ABC
CD4+	Rat	1:50	Dianova	Anti-Rat	1:250	ABC
CD11b+	Rat	1:50	Dianova	Anti-Rat	1:250	ABC
CD68+	Rabbit	1:150	EnVision	Anti-Rabbit	—	EnVision
Collagen I	Rabbit	1:500	EnVision	Anti-Rabbit	—	EnVision
Collagen III	Rabbit	1:200	EnVision	Anti-Rabbit	—	EnVision
Mcp-1	Rabbit	1:25	EnVision	Anti-Rabbit	—	EnVision

Pri.Ab=primary antibody, *Sec.Ab*=secondary antibody.

2.4.2.1 ABC method

The avidin-biotin complex method is triggered by the binding of an antibody to the appropriate target antigen and it is also known as the immuno-peroxidase method (Figure 5). The extraordinary affinity of avidin for biotin (over million times higher than the most physiological antibody-antigen affinity) allows specific binding between biotin-containing molecules and avidin in a complex mixture. This biochemical binding is one of the highest biological binding constants, and therefore has an almost irreversible character.

At first, the primary antibody binds to the corresponding antigen. Then, a biotinylated secondary antibody binds to the Fc fragment of the primary antibody. Subsequently, an enzyme (horse radish peroxidase (HRP) or alkaline phosphatase (AP)) mixed with avidin is added to form an avidin-biotin-enzyme complex on the slide, in which the ratio between the avidin and enzyme special remains to prevent avidin saturation. The addition of these enzyme-avidin mixtures produces an enzyme-substrate reaction between the remaining biotin-binding sites on the biotinylated secondary antibody. Following the addition of a carbazole solution (50 mg 3-amino-9-ethylcarbazole + 10 ml N, N-dimethylformamide + 15 ml 0.2 M acetic acid + 35 ml

0.2 M sodium + 100 µl 30% H_2O_2 diluted to 200 ml distilled water), the change in color will be visible. This method was used in this study to determine the infiltration of inflammatory cells such as CD3+, CD4+, and CD11b+.

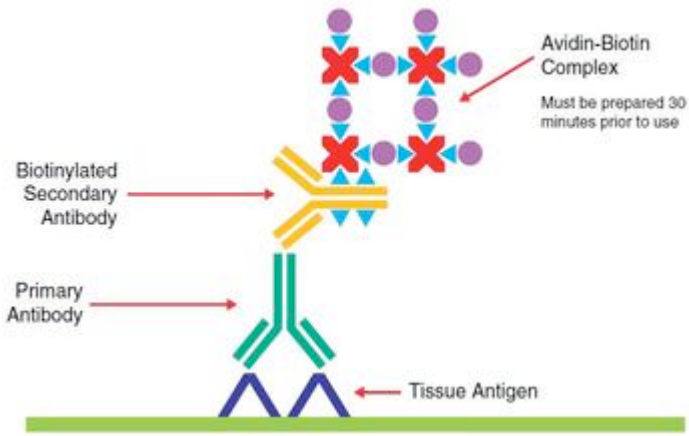

Figure 5. Schematic representation of the avidin-biotin complex (ABC) staining method (from George L. Kumar *et al.*[124]).

Procedure of the ABC method

All slides used for the staining were incubated in a cuvette, filled with 1×TBS, (a 10-fold dilution from 10×TBS: 60.6 g Trizma HCL + 13.9 g Trizma base + 87.66 g NaCl diluted to 1l pH 7.6-7.8 distilled water), for five minutes to adapt them to the buffer milieu. The effect of various endogenous peroxidases during the histological staining were blocked by immersion in 0.075% hydrogen peroxide solution (0.5 ml 30%H_2O_2 + 199.5 ml 1×TBS) for 7 minutes. Then, the slides were washed in 1×TBS for five minutes to clean the previously applied peroxide. To prevent nonspecific staining by the different electrostatic potential of proteins and to block endogenous avidin, all heart tissues were incubated in a blocking solution (10% normal serum, four drops of avidin, and 1% BSA pro milliliter 1×TBS) for 30 minutes at room temperature. Then, 100 µl solution (primary antibodies four drops of biotin, 1% BSA per milliliter 1×TBS) was added to each staining field. The slides were incubated for 60 minutes at room temperature to block the endogenous avidin and to bind the primary antibody. After that, the sections were washed two times for each five minutes in 1×TBS. Following this step, secondary biotinylated antibody was applied by dilution in 1×TBS and 1% BSA (100 µl 10%BSA + 896 µl 1×TBS + 4 µl secondary antibody). The tissue sections were incubated for 60 minutes to ensure the binding

of the secondary antibody to the primary antibody. Then, two washes were supplied in 1×TBS for each five minutes, and then the addition of the enzyme-avidin mixture (1ml 1×TBS + four drops of reagent A + four drops of reagent B) followed. An additional incubation was performed at room temperature for 30 minutes for building of the ABC-complex. Next, two washes of each five minutes in 1×TBS were performed. Following this, the peroxidase of the ABC complex reacted with the carbazole solution for 12 minutes, which resulted in the visual detection as red signals. After that, two washing processes of each five minutes in 1×TBS were repeated. The sections were counterstained by short-term immersion in Mayer's hematoxylin solution. Ultimately, after cleaning by tap water, all of the slides with stained myocardial sections were covered with glycerine gelatin and coverslipped.

In addition, a negative control of the staining was included. In each two respective negative staining fields, a buffer solution was used instead of the first antibody, so that the reaction of the secondary antibody to non-specific antigens, peroxidase, biotin and avidin block in tissues was excluded.

2.4.2.2 EnVision® detection method

The EnVision® method, a highly sensitive detection method, is applicable for a broad range of antibodies. This method is supported by the assistance of both enzymes and antibody-labeled polymer conjugates, whose biological structure contains a dextran backbone attached by multiple enzyme molecules (Figure 6). This staining method was used in this work to demonstrate the expression of collagen I, III, α-SMA, MCP-1 and CD68+ in the cardiac tissue seven days after infection.

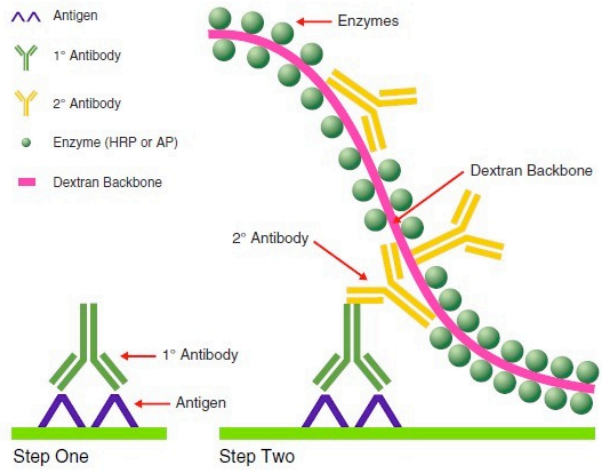

Figure 6. The 2-step Envision method includes the primary antibody (step 1) and dextranpolymer (step 2), which contains an average of 10 molecules of secondary antibodies and 70 molecules enzyme (from George L. Kumar *et al.*[124]).

Procedure of the EnVision® method

All slides used for the staining were incubated in a cuvette filled with 1×PBS (a 25-fold dilution from 25×PBS: 200 g NaCl + 5 g KCl + 6.25 g KH_2PO_4 + 33.75 g Na_2HPO_4*$2H_2O$ diluted to 1l pH 7.3 with distilled water), for five minutes, so that the heart histological sections on the slides could adapt to the buffer medium. Then, 0.075% hydrogen peroxide solution in 1×PBS was applied to block endogenous peroxidase. The previously applied peroxide on the histological section was then washed away in 1×PBS for five minutes. After that, a 1:500 primary antibody dilution buffer (from 9000 µl 1×PBS + 1000 µl 100% FCS) was applied to the staining fields. In the further course of the process, the sections were incubated in a humid chamber at room temperature for 60 minutes for the binding of the primary antibody to the protein. Then, two further washing processes of five minutes each in 1×PBS were performed. After addition of undiluted secondary antibody, the slides were incubated in a humid chamber for a further 30 minutes. This was followed by two washing processes in 1×PBS of five minutes each. Next, the carbazole solution was added. The cuvette was subsequently shaken on a shaker for 12 minutes. Sections were thereafter again washed two times in 1×PBS for 5 minutes each, and each slide was stained by sinking in hematoxylin for 30 seconds. In addition, the slides were rinsed with tap

water. Ultimately, all of the slides with stained myocardial sections were covered with glycerine gelatin and coverslipped.

As for the ABC-method, a negative control of the staining was also performed. All the tissue sections were stored at room temperature in the designated preparation box.

2.4.3 “DeadEnd Colorimetric TUNEL" system

The DeadEnd Colorimetric TUNEL detection system (Promega Corporation, Mannheim, Germany) provides a simple, accurate, and rapid detection of fragmented DNA in apoptotic cells. During this histochemical detection method, the Terminal Deoxynucleotidyl Transferase, Recombinant (rTdT) enzyme is used to incorporate biotinylated nucleotide at the 3'-OH DNA ends. After that, horseradish peroxidase-labeled streptavidin (Streptavidin HRP) will be bound to these biotinylated nucleotides. After the addition of carbazole, it can be detected visually.

Procedure of "DeadEnd Colorimetric TUNEL" system method

The DeadEnd Colorimetric TUNEL method used in this study was according to the protocol of Promega, only slightly modified. The samples were twice immersed in 1×PBS solution for a period of 5 minutes and then fixed with 10% buffered formalin for 15 minutes. Then, the slides were twice washed with 1×PBS for 5 minutes each. The cuvette of slides was supplemented with a 400 µl proteinase K buffer (500-fold from the solution of 10 mg/ml proteinase K + 5 ml 0.5 M EDTA+ 45 ml 100 mM Tris-HCL) and 200 ml 1×PBS, and incubated for 30 minutes at room temperature to expose the antigens on the tissue sections. After two washes of five minutes each in 1×PBS, all histological specimens were refixed with 10% buffered formalin. Two wash processes in 1×PBS were repeated.

Then, the tissue sections which served as positive controls were treated according to the following steps: DNAse I buffer (10 mM NaCl+ 6 mM $MgCl_2$+ 10 mM $CaCl_2$+ 40 mM Tris-HCl) was supplied for 5 minutes; 5-fold DNase I diluted in DNase I buffer was then added for ten minutes. Next, the sections were washed with distilled water for 3-4 times and immersed in 1×PBS for 5 minutes. By these steps, chromosomal DNA is destroyed enabling biotinylated nucleotides to bind.

All the slides were then covered with equilibration buffer and equilibrated at room temperature for 10 minutes. Subsequently, the slides were applied to the rTdT reaction mix (49 µl

equilibration buffer+ 0.5 µl biotinylated nucleotide mix+ 7.5 µl rTdT enzyme). For the negative control sections, the same volume of distilled water was added instead of the rTdT enzyme. All slides were then incubated for 60 minutes at a temperature of 37°C. The reaction was terminated by immersing the slides in 2×SSC for 15 minutes at room temperature. Furthermore, the wash process in fresh 1×PBS was repeated twice for each 5 minutes at room temperature to remove unincorporated biotinylated nucleotides. The function of the endogenous peroxidase was then blocked by 0.15% hydrogen peroxide solution for 3-5 minutes at room temperature, followed by two wash processes for each 5 minutes in fresh 1×PBS. Further, the binding reaction was carried out by adding 75 µl streptavidin HRP mix (1.5 µl stock solution of streptavidin HRP was diluted to 750 µl 1×PBS to each ten slides) over 30 minutes at room temperature. The sections were washed in 1×PBS twice for each five minutes. Then the carbazole solution was added for 12 minutes. Following the above-mentioned staining procedures, the sections were counterstained by sinking in hemalum and all slides were covered with glycerine gelatin.

2.4.4 The method of color-coded and image analysis

All tissue sections were analyzed by light microscopy without knowing the record number of the group, and were analyzed with the color-coded digital image analysis technique. 20 view fields from each specimen were evaluated in a 200-fold magnification and digitized by a video camera. The pictures were recorded in a 704 x 548 pixel RGB format with color quality of 16 bit. With this evaluation method, the selected fields in light microscope will be evaluated independently and accurately. The digital image processing was performed with the digital software Lucia G for which a self-programmed macro, one for areal and one for cell calculation, had been developed.

The procedure takes place in four steps:

- Digital acquisition and sharpening and contrasting the picture in real time
- Manual selection of the receiving surface by using the image analysis program. The size of the measured area is confirmed.
- Automatic measurement of three separate areas:

  Measurement of the selected area (A_M).

  Measurement of the background area which was not covered by tissue (A_H).

Measurement of areas which had been stained (A_A).

- The results of the measured fields of heart muscle section were exported from the image analysis program to a data analysis Microsoft Excel macro, which calculates the expression of antigens per cardiac muscle tissue area according to the following formula:

$$E_A = \sum_{1-n}^{n} \frac{A_A}{A_M - A_H}$$

n = number of the fields; [EA] = mm^2/mm^2.

All microscopic images obtained for detecting the stained antigens were measured with a 200-fold microscope magnification. Quantification of collagen I, collagen III, MCP-1, α-SMA was expressed in area fraction ("area fraction" in%, AF). The infiltrative immune cells, CD3+, CD4+, CD11b+, CD68+, are evaluated in the form of positive cells/mm^2.

3. Results

3.1 Body and heart weight

It was found that the body weight (BW) of mice, which were infected with CVB3, was reduced seven days after infection compared with the BW of non-infected mice of the same strain.

The NOD2$^{-/-}$CVB3 mice had a significantly lower heart weight (HW)/BW ratio compared to the WT-CVB3 (Table 10). Furthermore, a significant reduction in BW in the infected groups compared to the uninfected control groups (Table 10) was observed. There was no significant difference in BW and HW between the NOD2$^{-/-}$CVB3 mice and the WT CVB3 mice.

Table 10. Body and heart weight

	WT	**NOD2$^{-/-}$**	**WT CVB3**	**NOD2$^{-/-}$CVB3**
BW*(g)*	23.84±1.61	23.1±1.21	20.36±2.72*	20.73±1.42$^{\#}$
HW*(mg)*	115.86±10.65	113.67±11.41	112.44±14.58	104.44±7.18
HW/BW*(mg/g)*	4.86±0.26	4.91±0.29	5.54±0.31*	5.04±0.28$^{\$}$

All values are expressed as mean ± standard deviation. (*BW* = body weight, *HW* = heart weight, *p<0.05 vs WT mice, #p<0.05 vs NOD2$^{-/-}$ mice, $p<0.05 vs WT CVB3 mice).

3.2 Hemodynamic function

The hemodynamic data of the WT CVB3 group showed unimpaired LV systolic function in comparison with the non-infected WT mice seven days after CVB3 infection, defined by a reduced maximum LV pressure (61.29±2.56 vs 73.55±4.36 mmHg, p<0.05), minimum LV pressure (1.60±0.25 vs. 2.31±0.19 mmHg, p<0.05), end-systolic LV pressure (49.60±1.78 vs. 62.32±3.50 mmHg, p<0.05), and dP/dt_{max} (5069±342.9 vs. 6569±755.5 mmHg/s, p<0.05). The reductions in EF value were less pronounced in NOD2$^{-/-}$CVB3 mice compared to WT CVB3 mice (p<0.05) (Table 11).

Left ventricular diastolic function in WT CVB3 group was significantly impaired compared to NOD2$^{-/-}$CVB3 mice as indicated by a reduced end-diastolic LV pressure (4.26±0.35 vs. 4.52±0.58 mmHg, p<0.05), and a higher dP/dtmin (-3228±239.4 vs. -4215±182.9 mmHg/s, p<0.05) (Table 11).

Table 11. Hemodynamic parameter seven days after infection

	WT	**NOD2$^{-/-}$**	**WT CVB3**	**NOD2$^{-/-}$CVB3**
Global cardiac function				
HR*(bpm)*	526.9±29.21	568.1±16.58	521.1±13.09	528.2±14.08
LVESV*(µl)*	33.15±2.03	29.09±1.65	30.86±4.47	31.20±1.32
LVEDV*(µl)*	77.89±7.17	72.59±5.03	75.05±12.79	79.42±4.62
SV*(µl)*	47.18±4.92	49.88±3.63	37.51±5.83	51.71±3.75
CO*(µl/min)*	24270±8657	27553±7150	22417±13782	27060±4872
EF*(%)*	60.13±1.04	61.89±2.66	55.42±1.80	64.64±1.41$^{\$}$
Systolic function				
LVPmax*(mmHg)*	73.55±4.36	76.28±2.71	61.29±2.56*	71.05±2.52$^{\$}$
LVP_{min}*(mmHg)*	2.31±0.19	2.25±0.27	1.60±0.25*	1.37±0.43
LVESP*(mmHg)*	62.32±3.50	63.78±3.26	49.60±1.78*	57.11±1.99
dP/dt_{max}*(mmHg/s)*	6569±755.5	6938±553.4	5069±342.9*	5980±453.8
Diastolic function				
LVEDP*(mmHg)*	4.07±0.31	5.24±0.65	4.26±0.35	4.52±0.58$^{\$}$
dP/dt_{min}*(mmHg/s)*	-4481±438.2	-4504±258.9	-3228±239.4	-4215±182.9$^{\$}$
Tau*(ms)*	10.46±1.02	9.28±0.44	9.64±0.55	8.97±0.33

All values are expressed as the mean ± standard deviation. (*LVESV* = end-systolic LV volume, *LVEDV* = end-diastolic LV volume, *SV* = stroke volume, *CO* = cardiac output, *EF* = ejection fraction, LVP_{max} = maximum LV pressure, *LVESP* = end-systolic LV pressure, dP/dt_{max} = maximal LV pressure rise rate, *LVEDP* = end-diastolic LV pressure, LVP_{min} = minimum LV pressure, dP/dt_{min} = maximum LV pressure drop rate, *Tau* = time of the LV pressure decrease, *p<0.05 vs. WT mice, #p<0.05 vs. NOD2$^{-/-}$ mice, $p<0.05 vs. WTCVB3 mice).

3.3 Hematoxylin staining of viral myocarditis

We examined the morphology of left ventricular tissue by hematoxylin eosin (HE)-staining to obtain an overview of the pathological changes in the cardiac tissue.

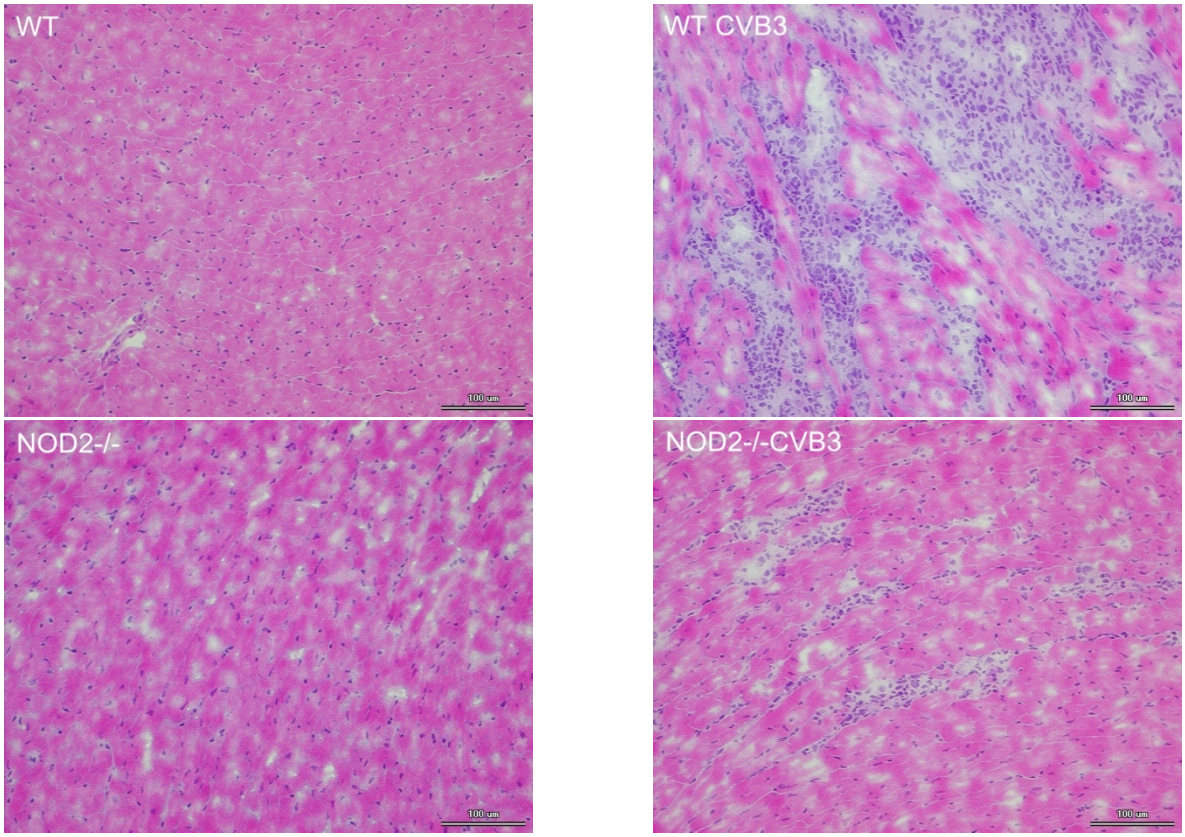

Figure 7. Representative hematoxylin eosin-stainings in the left ventricle of WT, WTCVB3, NOD2-/-, and NOD2-/-CVB3 mice . 200×magnification. WT = wild-type, CVB3 = coxsackie virus B3.

3.4 Inflammation

3.4.1 Immune cell infiltration

The number of migrating cells was immunohistochemically examined using specific markers for the different cell types. CD3+, CD4+ were used as a marker for all T cells, CD11b+ for T-cells and macrophages, CD68+ for macrophages. Both infected groups showed increased infiltration of CD3+, CD4+, CD11b+ and CD68+ cells in the myocardium compared to the respective healthy control animals ($P < 0.05$). The number of these cell types in the WT-CVB3 mice was significantly higher than in the $NOD2^{-/-}$CVB3 mice ($P<0.05$) (Figure 8). It demonstrated that immune cell infiltration seven days after infection was less pronounced in the heart tissue of

NOD2$^{-/-}$CVB3 mice compared to WT-CVB3 mice.

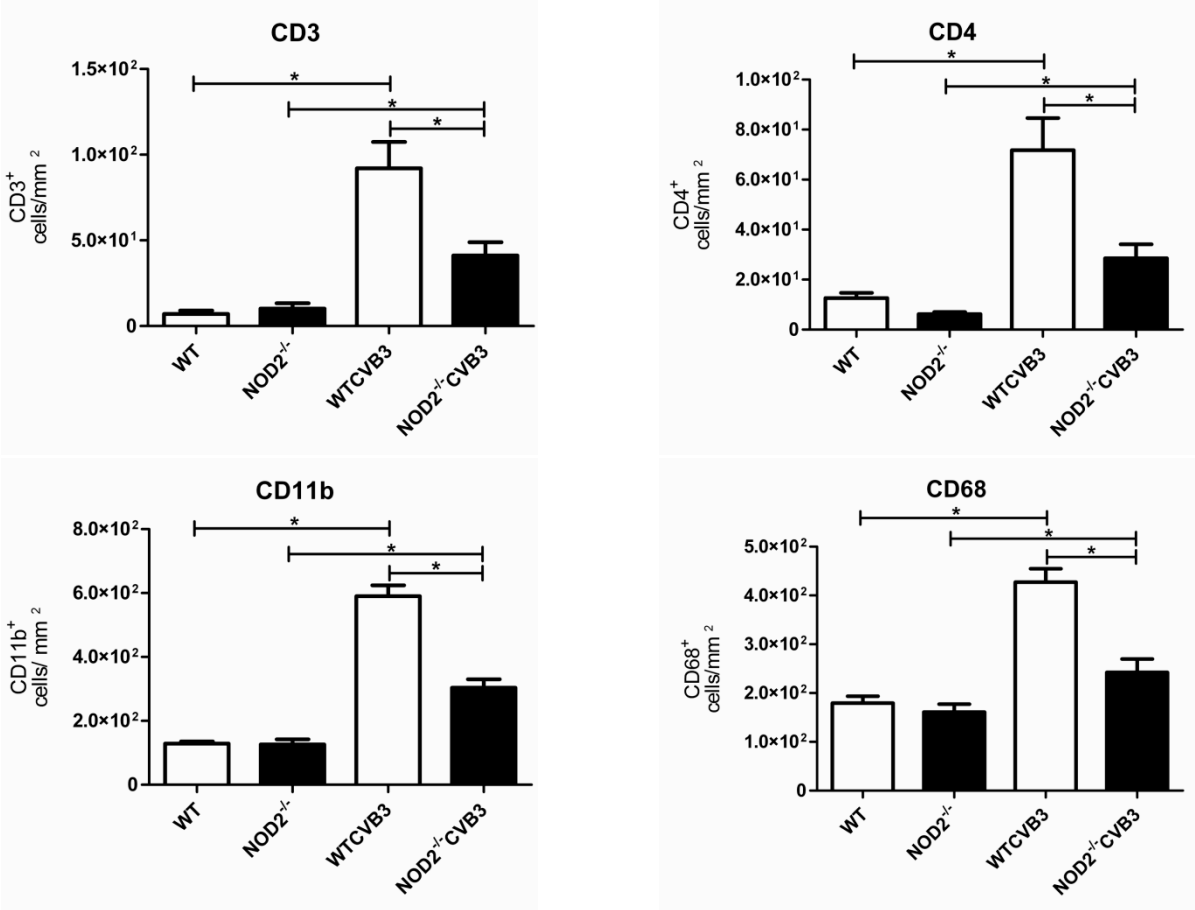

Figure 8. Left ventricular presence of CD3+ T lymphocytes (top left), CD4+ activated T lymphocytes (top right), CD11b+ T lymphocytes and macrophages (bottom left) and CD68+ macrophages (bottom right) seven days after CVB3 infection, collected using specific immunohistochemistry and quantified by digital image analysis, are shown. Seven days after viral infection, NOD2$^{-/-}$CVB3 and WT-CVB3 groups showed exacerbation of cardiac infiltration of immune cells compared to their respective control mice. left ventricular presence of CD3+, CD4+, CD11b+, and CD68+ cells was all significantly lower in NOD2-/-CVB3 mice than in WT-CVB3 mice (*= $p<0.05$). All data are reported as the mean value (MV) ± standard error of the mean (SEM). WT = wild-type, CVB3 = coxsackie virus B3.

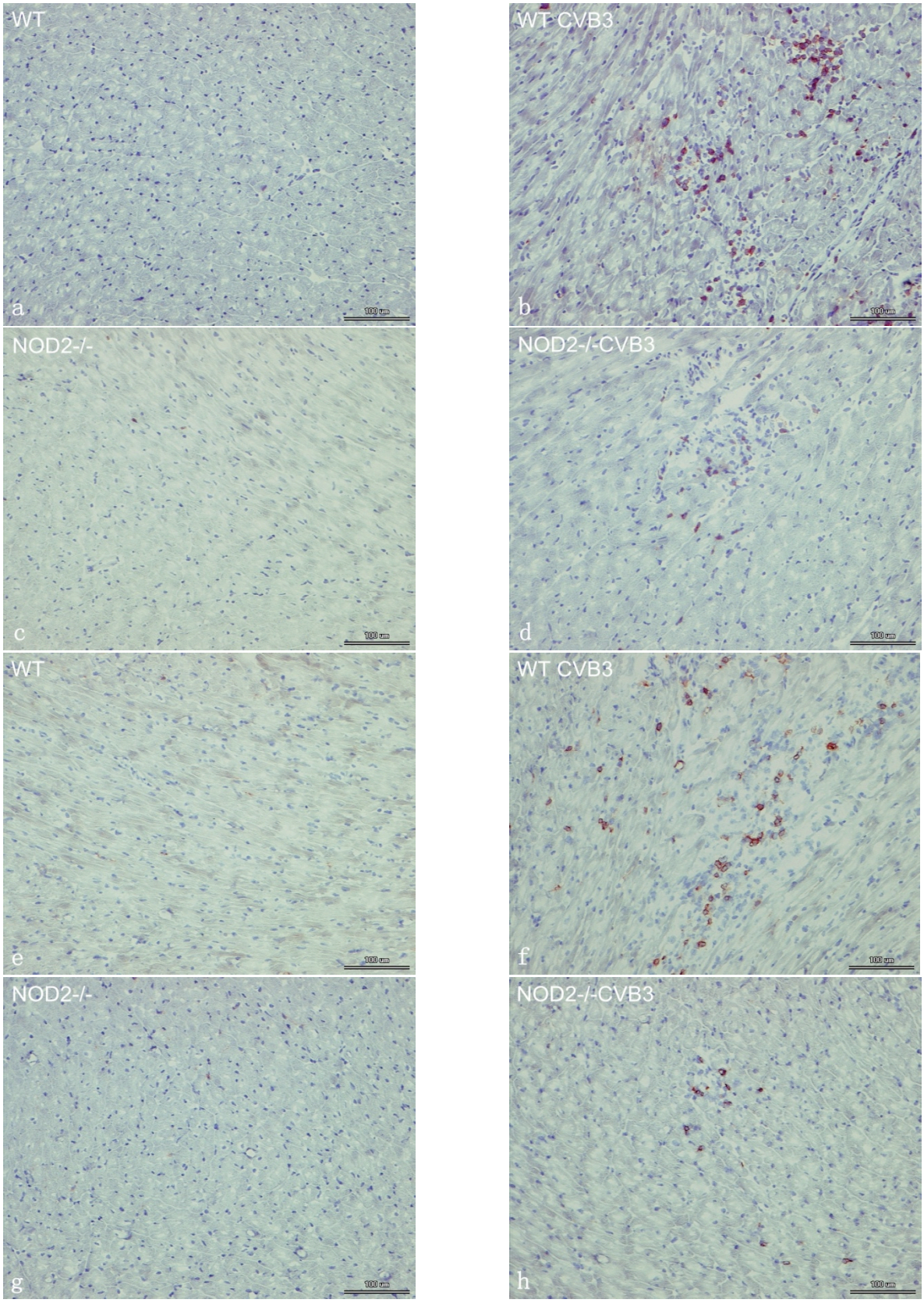

Figure 9. Representative immunohistochemical stainings of CD3+ (a to d) and CD4+ (e to h) T lymphocytes in the left ventricle. 200×magnification. Specific epitopes are stained red.